University of Thessaly
School of Engineering
Department of Mechanical Engineering

Master of Science

Analytical and Numerical methodologies for the analysis and design of pipelines crossing seismic faults

by

Gregory Sarvanis
Diploma of Civil Engineering, U.th.

Supervisor: Prof. Spyros A. Karamanos

Submitted to
the department of Mechanical Engineering
in Fulfillment of the requirements
for the Degree of Master of Science

Volos 2015

Πανεπιστήμιο Θεσσαλίας
Πολυτεχνική Σχολή
Τμήμα Μηχανολόγων Μηχανικών

Μεταπτυχιακό Δίπλωμα Ειδίκευσης

Αναλυτικές και αριθμητικές μέθοδοι για την ανάλυση και τον σχεδιασμό υπόγειων χαλύβδινων αγωγών οι οποίοι διέρχονται απο σεισμικά ρήγματα.

Σαρβάνης γρηγόρης

Διπλωματούχος Πολιτικός Μηχανικός, Π.Θ.

Επιβλέπων: Καθ. Σπύρος Α. Καραμάνος

Υπεβλήθη για την εκπλήρωση μέρους των
απαιτήσεων για την απόκτηση του
Μεταπτυχιακού Διπλώματος Ειδίκευσης

Βόλος 2015

Examination committee:

Dr. Spyros A. Karamanos, Professor, Department of Mechanical Engineering, University of Thessaly.

Dr. Panos Dakoulas, Professor, Department of Civil Engineering, University of Thessaly.

Dr. Gregory N. Haidemenopoulos, Professor, Department of Mechanical Engineering, University of Thessaly.

Analytical and Numerical methodologies for the analysis and design of pipelines crossing seismic faults

Gregory Sarvanis

University of Thessaly, Department of Mechanical Engineering

Supervisor: Prof. Spyros A. Karamanos

Abstract

Buried pipelines often cross geohazard areas such as seismic faults and liquefied areas. In the present work analytical and numerical methodologies are investigated and compared. Two analytical methodologies are analyzed, proposed by Kennedy et al. (1977) and by Vazouras et al. (2012) while a new methodology for analyzing buried pipelines which cross seismic faults is proposed and compared with results from finite element analysis, commercial codes and methodologies from the literature. Moreover the pipe-soil interaction is investigated through the numerical simulation of several experimental tests, which have been conducted in the framework of a European research program (GIPIPE). The experiments are concern pipes embedded in soil, subjected to loading in the axial and the transverse direction as well as a complex scenario of loading simulating the conditions during a severe lateral loading of a pipeline due to strike-slip fault of a landslide. All these tests have been conducted at CSM facilities in Sardinia.

Αναλυτικές και αριθμητικές μέθοδοι για την ανάλυση και τον σχεδιασμό υπόγειων χαλύβδινων αγωγών οι οποίοι διέρχονται απο σεισμικά ρήγματα.

Σαρβάνης γρηγόρης

Πανεπιστήμιο Θεσσαλίας, Τμήμα Μηχανολόγων Μηχανικών

Επιβλέπων: Καθ. Σπύρος Α. Καραμάνος

Περίληψη

Οι υπόγειοι αγωγοί συχνά διέρχονται από περιοχές αυξημένων σεισμικών κινδύνων όπως τα σεισμικά ρήγματα, οι ρευστοποιήσιμες περιοχές καθώς και οι περιοχές κατολισθήσεων. Στην παρούσα εργασία εξετάσθηκαν δύο αναλυτικές μέθοδοι για την ανάλυση υπόγειων αγωγών, η μεθοδολογία των Kennedy et al. (1977) και των Vazouras et al. (2012), ενώ αναπτύχθηκε μια νέα απλοποιημένη μεθοδολογία για την ανάλυση υπόγειων χαλύβδινων αγωγών οι οποίοι διασταυρώνονται από σεισμικά ρήγματα. Επίσης μελετήθηκε η αλληλεπίδραση αγωγού-εδάφους μέσα από την προσομοίωση πειραμάτων τα οποία πραγματοποιήθηκαν στα πλαίσια του ερευνητικού προγράμματος (GIPIPE). Τα πειράματα αφορούν θαμμένους αγωγούς οι οποίοι υποβάλλονται σε αξονική και εγκάρσια φόρτιση καθώς και σε μια συνδυασμένη φόρτιση η οποία προσομοιώνει συνθήκες κατολίσθησης. Το σύνολο των πειραμάτων πραγματοποιήθηκε στις εγκαταστάσεις του CSM, στην Σαρδηνία.

Table of contents

1. Introduction

1.1 Description of physical problem

An earthquake is characterized by ground shaking often caused by an abrupt shift of rock along a fracture in the Earth, called a fault. The tectonic plates make up the slow-moving outer shield of Earth and often stick due to friction. As pressure builds up from trying to move, the stress increases. When the stress overcomes the friction at the interface, i.e. the fault surface, an earthquake occurs; the plates quickly move relatively and because the friction energy is released into the crust. The energy released is transmitted through the ground and causes shaking associated with an earthquake. Figure 1 demonstrates rupture expansion during a severe earthquake. The images in Figure 1 depict the sequence of events along a fault plane as the rupture expands and seismic waves are radiated when an earthquake occurs. The friction across the surface of the fault holds the rocks together so that they tend to slip when pushed. Eventually enough stress builds up and brittle failure caused the rocks to slip suddenly, releasing energy in the form of seismic waves that propagate along the entire length of the fault until the earthquake stops. The hypocenter, defined as the point on the fault plane where the earthquake begins, is located usually at a certain depth beneath the fault, while the epicenter is the point directly above the hypocenter, on the fault surface. The "focus" in the Figure 1 is the hypocenter, the epicenter would be the point directly about the "focus" but on the fault surface.

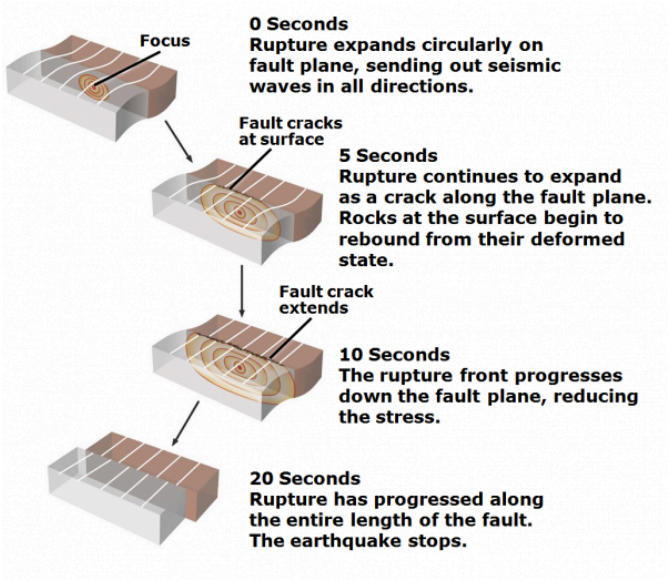

Figure 1. Fault rupture expansion during a large earthquake (www.scec.usc.edu).

Based on the above, faults can be considered essentially as cracks in layers of rock, along with the relative displacement of the fault. The relative displacement of the two parts of the ground is called fault slip. After a fault has slipped, due to the release of stress, it locks up again. The steady movement of the rocks on either side of the fault causes the stresses to begin to rise again, and the cycle repeats. The length of a fault can range anywhere from a few millimeters to thousands of kilometers. The fault surface can be vertical, horizontal, or at some angle with respect to ground surface. They can extend well into the Earth and may also extend to the surface. They can be categorized into four different fault types: Normal, Reverse, Strike-Slip, and Oblique as shown on Figure 2. Normal faults are characterized by the foot-wall moving up in relation to the hanging-wall, as shown in Figure 2. Reverse faults have an "opposite" configuration of normal faults. They occur when the hanging-wall move up in relation to the foot-wall. Sometimes, reverse faults are also referred to as "Thrust faults". Strike-slip faults can be divided in two categories the left-lateral strike-slips faults and the right-lateral strike slips faults. Left-lateral strike-slip faults occur when the two side move parallel to one another. There is no vertical displacement, only horizontal. In order to identify whether a fault is left-lateral, when standing on one side and looking to the fault, the other side of the fault has apparent displacement to the left. Right-lateral strike-slip faults have the same motion as left-lateral, however, if standing on one side of the fault and looking to the fault, the other side appears to have moved to the right. The most famous fault in California, the San Andreas fault, is a right-lateral strike-slip fault.

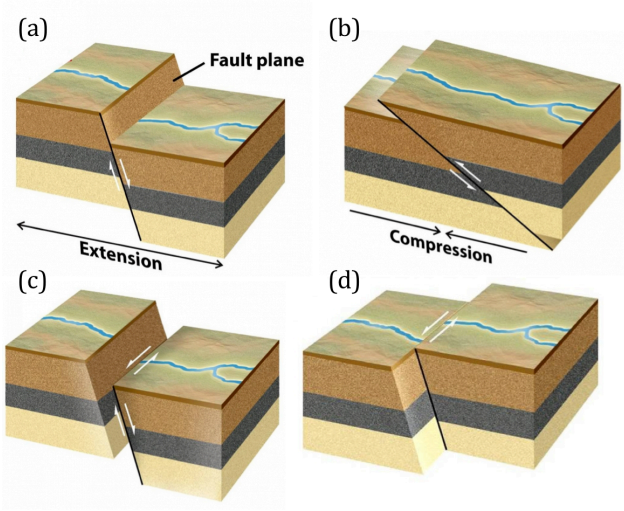

Figure 2. Different fault types, (a) Normal fault, (b) Reverse fault, (c) Oblique fault, (d) Strike-slip fault (www.scec.usc.edu).

Buried pipelines often cross tectonically active areas such as Greece, North Turkey, Nepal or California and may cross active faults capable of producing large earthquakes and large ground deformations. Avoiding crossing with seismic faults is the safer design option but this is not always possible. In Figure 3 the faults density along a buffer zone of width 2 kilometers in the area of Evros, North-East Greece, is shown. If a pipeline alignment falls within this buffer zone, then it will cross most of these faults. In such a case the pipeline must be designed, taking into account the extra stress and deformation induced by the pipe due to fault movement. In Figure 4 the pipeline deformation due to the movement of different types of seismic faults is shown. In the case of a normal fault, the pipeline is under tension and bending while in the case of a reverse fault the pipeline is under compression and bending which is most critical for local buckling failure. The crossing angle in the case of a strike-slip fault dictates whether the pipeline is under tension or compression. Therefore the choice of the crossing angle is a design parameter to be considered.

In the present work analytical and numerical methodologies are investigated and compared. In particular two analytical methodologies are analyzed in chapter 2, proposed by Kennedy et al. (1977) and by Vazouras et al. (2012). Also a new methodology for analyzing buried pipelines which cross seismic faults is proposed and compared with results from finite element analysis, commercial codes and methodologies from the literature. Moreover the pipe-soil interaction is investigated through the numerical simulation of several experimental tests, which have been conducted in the framework of a European research program (GIPIPE). The experiments are concern pipes embedded in soil, subjected to loading in the axial and the transverse direction as well as a complex scenario of loading simulating the conditions during a severe lateral loading of a pipeline due to strike-slip fault of a landslide. All these tests have been conducted at CSM facilities in Sardinia.

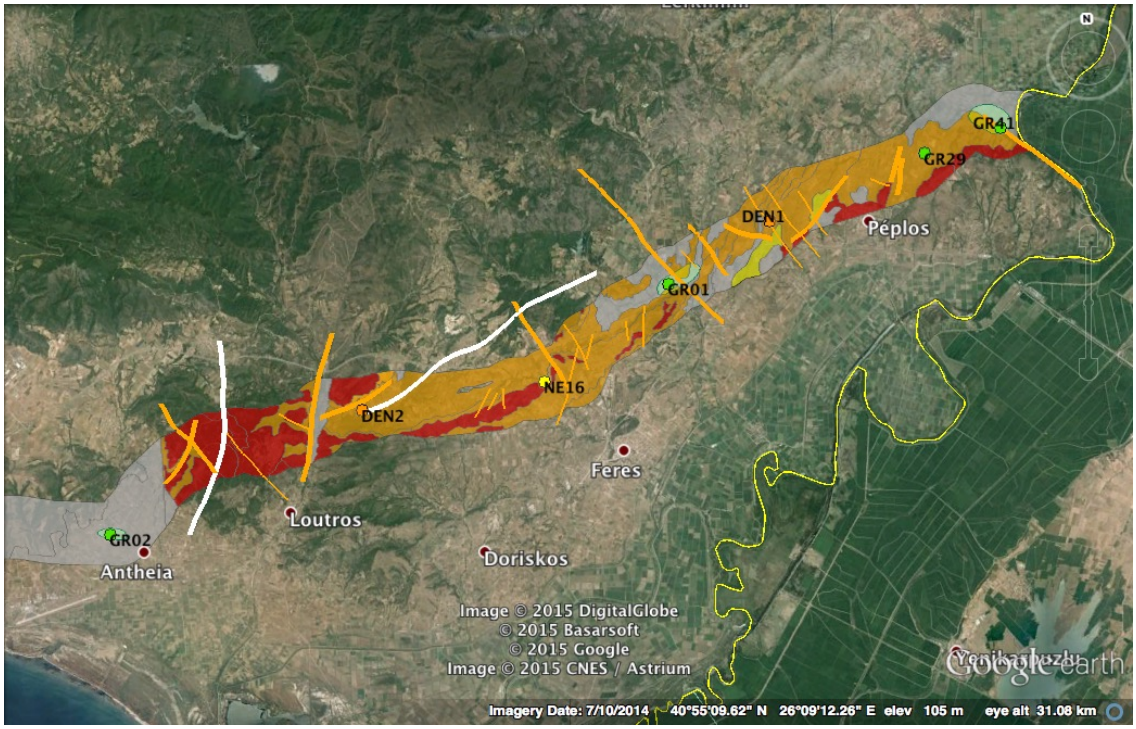

Figure 3. Fault density along a buffer zone of 2 kilometers width, around a pipeline in the area of Evros.

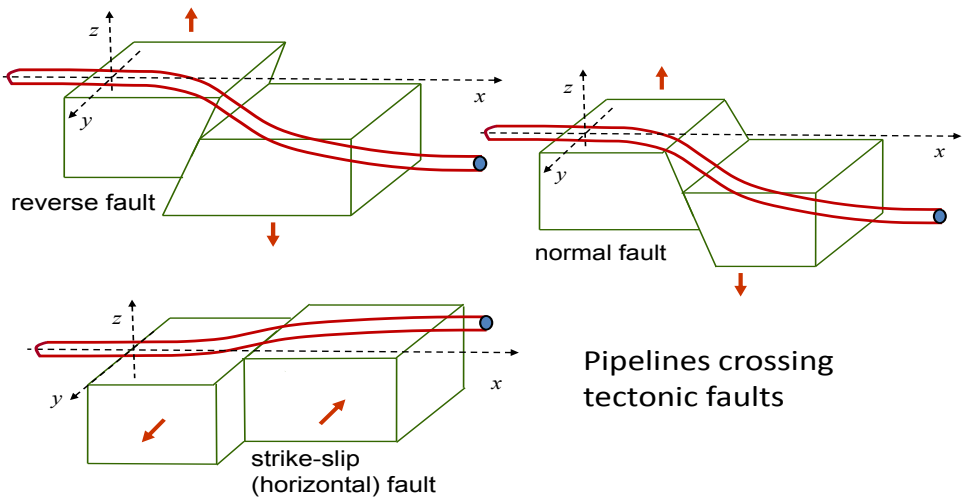

Figure 4. Pipeline deformation due to the movement of different types of seismic faults (GIPIPE).

1.2 Pipeline accidents due to earthquake action

There are various examples of earthquakes that have caused severe damage to buried pipelines, such as the earthquakes of San Fernando 1971, Managua 1972, Haicheng 1975, Tang-shan 1976, Miyagiken-Oki 1978, Northridge 1994, Kobe 1995, Chi-Chi 1999, Kocaeli 1999 and more recently Chile 2010, Christchurch 2010-2011, and

Japan 2011. Table 1 shows a list of various North American earthquakes for which pipeline damage have been documented by O' Rourk and McCaffrey. In most instances, pipeline damage has been attributed to permanent ground movements.

Table 1. Summary of North American earthquakes with significant reported pipeline damage.

Earthquake	**Magnitude**	**Permanent Ground Movement**	**Damages**
1906 San Francisco	8.3	Strike-slip faulting with max disp. 6.4 m, extensive slope stability problems, lateral spread and flow failures	Water pipelines rapture at 9 locations along San Andreas fault, extensive damage to water and gas pipelines due to liquefaction- induced movements
1931 Managua	Not reported	One main zone of faulting, landslides along steep natural slopes	Principal water main for Managua ruptured at fault. Steel pipeline ruptured by landslide
1933 Long Beach	6.3	Ground cracks with seeping water, sand boils and local subsidence	Over 500 pipelines breaks, greatest concentration of pipelines failure near bays, rivers and flood control channels.
1952 Kern Country	7.7	Reverse oblique surface faulting. Many landslides.	Oil pipelines rupture along western extension of surface faulting, gas transmission line deformed but no rupture at fault crossing
1964 Alaska	8.4	Two reverse faults. Extensive landslides and submarine slope failures. Lateral spreads and flow failures	Over 200 breaks in gas and 100 breaks in water pipelines in Anchorage.
1971 San Fernando	6.4	Reverse oblique surface faulting. Over 1000 landslides and lateral spreads.	Over 2400 breaks in water, gas and sewage pipelines. Majority failures at faults and lateral spreads.
1972 Managua	5.6	Four main surface fault with max strike slip disp. of 0.4 m. Landslides along steep natural slopes.	Extensive damage to water distribution system. Many pipelines rupture at fault crossing

1.3 Literature review

The publication of Newmark and Hall (1975) has been pioneering in this area introducing an analytical model for assessing the integrity of a buried pipeline crossing a ruptured fault. Their model was based on the assumption of a single fault plane by considering soil masses on both fault sides as rigid bodies. They introduced the concept of "anchor point" situated at a certain distance from the fault, beyond which the pipeline and the surrounding soil have relative displacement equal to zero. Continuing the work of Newmark and Hall (1975), Kennedy et al. (1977) developed an analytical model, considering a non-uniform friction interface between the pipe and the soil, which was assumed to be cohesionless. This methodology is analyzed in detail in chapter 2.4 and compared with other methodologies. Wang and Yeh (1985) improved this methodology accounting for pipeline bending stiffness. This methodology considers a division of the pipe into four segments, as shown in Figure 5. The two pipe segments at the two ends behave as beams on elastic foundation, whereas the two inner segments have a constant curvature.

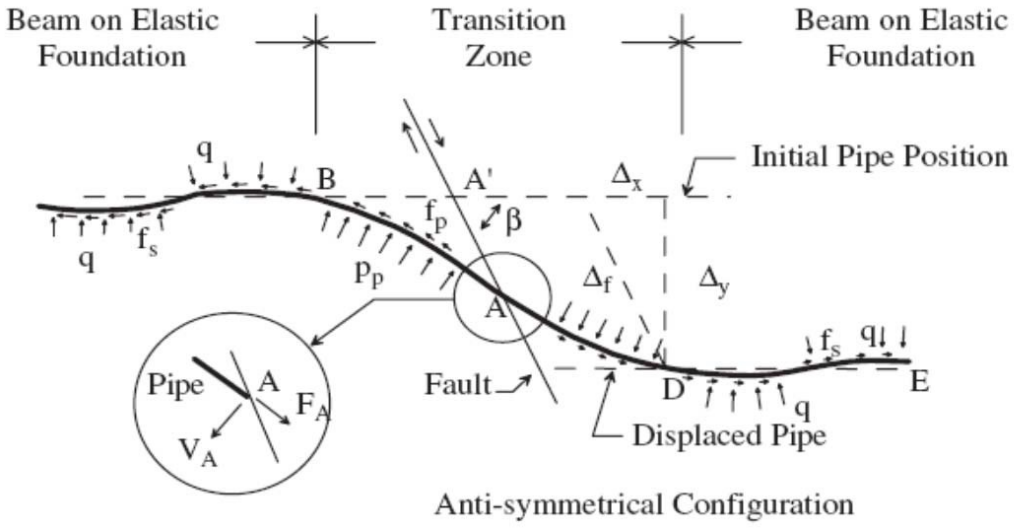

Figure 5. Model proposed by Wang and Yeh (1985).

Wang and Wang (1995) studied the problem considering the pipe as a beam on elastic foundation, whereas Takada et al. (2001) presented a new simplified method for evaluating the critical strain of the fault crossing steel pipes using relation between pipe longitudinal deformation and cross-sectional deformation. Karamitros et al.

improved analytical methodologies for strike-slip and normal faults by combining the theory of beam-on-elastic-foundation and the elastic-beam theory to calculate the bending moments. Trifonov et al. (2010 and 2012) improved the pipeline stress analysis using a semi-analytical approach. Vazouras et al. (2010 and 2012) studied the problem throw a rigorous numerical model which employ four-node reduced integration shell elements (type S4R) for the modeling of cylindrical pipeline segment and eight-node reduced-integration "brick" elements (C3D8R) for the simulation of the surrounding soil. The mechanical behavior of soil material is described through the Mohr-Coulomb model. In Figure 6 the mesh and the dimensions of the model are illustrated for a case of a 36-in-diameter pipe (diameter equal to 914.4 mm) for the case where, the pipeline is perpendicular to the fault plane. Vazouras et al. (2012) also proposed an analytical model for strike-slip faults, this methodology is analyzed in chapter 2.5.

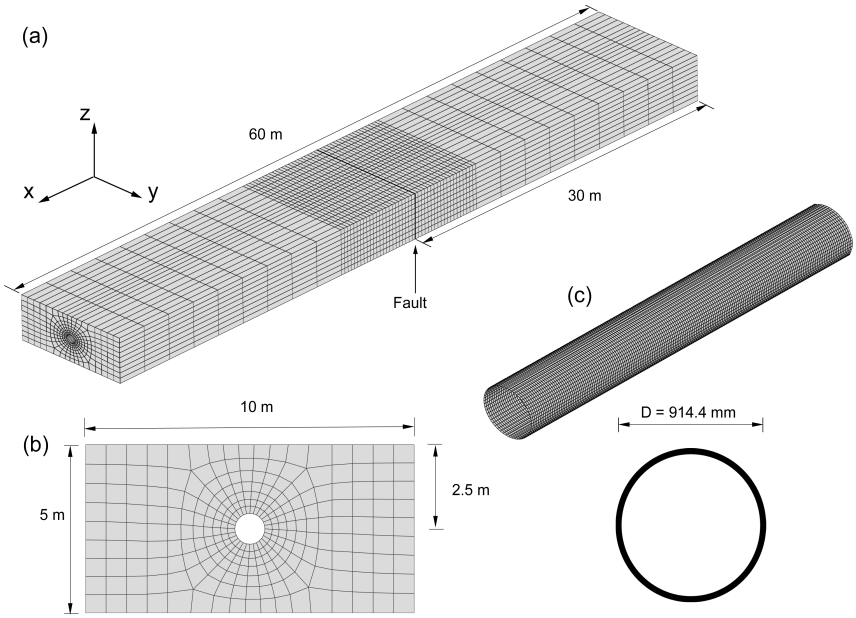

Figure 6. Finite element model as developed by Vazouras et al.

As far as pipe-soil interaction there are limited experimental tests in the literature. The work of Trautmann and O'Rourke (1985) has been pioneering in this type of experimental testing. In that paper the effects of pipe depth, soil density, pipe diameter and pipe roughness on the lateral force-displacement response of buried pipelines has been examined. Other experiments related to this subject were performed by Paulin et al. (1998) and Anderson et al. (2004). More lately, Karimian

(2006) reported the performance of experimental testing for axial and transverse response of buried pipelines. Very recently, in the framework of the GIPIPE project, a series of tests had been performed by CSM with the aim at examining experimentally soil-pipeline interaction under ground-induced actions. In particular, three pull-out and three transversal tests conducted in order to identify pipe-soil interaction in the axial and the transversal direction, respectively. Those tests have been performed mainly with the purpose of calibrating numerical finite element models. Moreover four large-scale landslide/fault tests have been performed in order to investigate the complex pipe soil interaction in a more realistic scenario. In Table 1, details on the experimental testing parameters are presented for the axial, transversal and landslide tests. In all cases, the diameter of pipe specimens is equal to 219.6 mm (8-inch-diameter pipes), the wall thickness is equal to 5.56 mm and the steel grade is API5L X65.

Table 2. Information about experimental testing conducted by CSM.

Test	Compaction Level D_r (%)	Mass density (Kg/m^3)	Water content (%)	Coating	Internal pressure (MPa)
Axial 1	40	1629	5.7	Bare	0
Axial 2	20	1602	7.8	Bare	0
Axial 3	40	1613	5.8	Coated	0
Transversal 1	20	1601	7.6	Bare	0
Transversal 2	40	1640	6.1	Bare	0
Transversal 3	40	1645	7.3	Coated	0
Landslide 1	40	1600	8.0	Bare	0
Landslide 2	40	1688	-	Bare	11.4
Landslide 3	20	1600	-	Bare	0
Landslide 4	20	1600	-	Bare	11.4

2. Simplified Models and Analytical Methodologies

2.1 Introduction

Simplified analytical equations and methodologies are presented for describing buried pipeline deformation under severe permanent ground-induced actions. Some methodologies have been proposed elsewhere, whereas an analytical methodology for strike-slip fault crossing has been developed in the course of GIPIPE. Those methodologies have been the only tool for the analysing buried pipelined under permanent ground-induced actions in the 70's and 80's, but they are also used presently in a more enhanced form. In their original form they are based on elastic beam or cable theory and are capable at estimating the stresses and strains that develop in the pipeline as well as the deformation state of the pipeline.

The design approach that uses analytical equations/methodologies is basically employed for a preliminary design stage. With this approach, a first understanding of various parameters can be obtained. In any case, a more rigorous approach with Finite Elements (either with beam-type element and soil springs, or in very specific cases, with three dimensional shell and solid elements) should be adopted for the detailed stress analysis and design of the pipeline.

2.2 Commercial design standards and recommendations for buried pipelines

The following standards and publications are relevant to the response of buried pipelines in permanent ground-induced actions such as seismic faults and landslides due to liquefaction or slope instability.

EN 1594: Gas supply sytems-Pipelines for maximum operating pressure over 16 bar

EN1998-4 (Eurocode 8): Design of structures for Earthquake resistance - Part 4: Silos, Tanks and Pipelines

EN 14161: Petroleum and natural gas industries- Pipeline transportation systems

ALA (2001): American Lifelines Alliance: Guidelines for the design of buried steel pipe, 2001.

ALA (2005): American Lifelines Alliance: Seismic Guidelines for Water Pipelines, 2005.

NEN 3650-1: Requirements for Pipeline systems, part 1

NEN 3650-2: Requirements for Pipeline systems, part 2

ASME B31.4: Pipeline transportation systems for liquid Hydrocarbons & other liquids

ASME B 31.8: Gas transmission and distribution piping systems

The methodologies and formulae for the response of buried pipelines according to ALA (2001) are presented for all types of permanent soil displacement. The response of a buried pipe to longitudinal and transversal permanent ground displacement as well as the pipe response in the case of a fault crossing are analyzed below.

Liquefaction or Landslides

- *Buried Pipe Response to Longitudinal PGD*

There are cases where the PGD, caused by a liquefaction or landslide, occurs in the longitudinal direction of the pipeline as shown in Figure 7. In those cases, a soil mass of length L_s is moving and applies axial force to the pipe as it moves in the longitudinal direction.

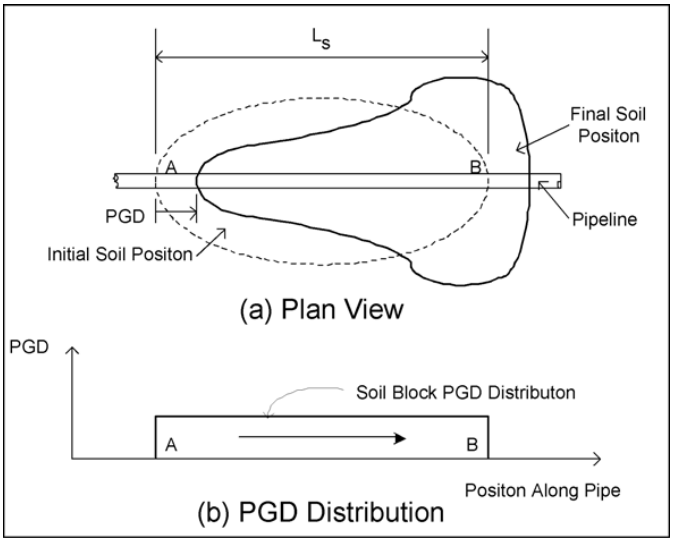

Figure 7. Schematic representation of ground action and pipe loading due to longitudinal PGD (ALA 2001).

For continuous buried pipes subjected to longitudinal permanent ground deformation, the axial forces F_1 and F_2 should be computed, representing upper-bound estimates of the axial force transmitted in the pipe by the moving soil. In particular F_1 is the force computed assuming that the pipe is elastic and fully compliant with the soil and F_2 is the ultimate force that the soil can transfer to the pipe due to the strength of the soil/pipe frictional interface.

$$F_1 = \sqrt{AEt_u\delta} \qquad \text{Eq. 1}$$

$$F_2 = \frac{t_u L_s}{2} \qquad \text{Eq. 2}$$

In the above expression, t_u is the maximum soil resistance to the pipe axial direction per unit length of pipe and δ is the expected value of the PGD under consideration. The force for designing the buried pipe should be taken as the smaller of forces F_1 and F_2.

- *Buried Pipe Response to Transverse PGD*

Permanent ground deformation due to landslide or liquefaction can also occur in the transverse (horizontal) direction of the pipeline. In this case, a soil mass of length W moves in the transverse direction of the pipeline as shown in Figure 8.

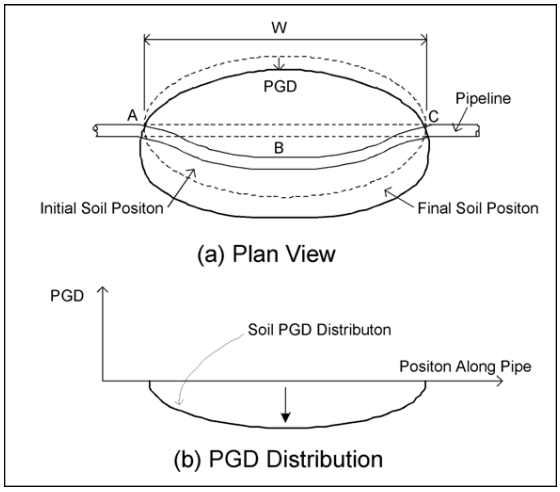

Figure 8. Schematic representation of ground action and pipe loading due to to transverse PGD (ALA 2001)

Estimates of the ground-induced bending strains in the case of a buried pipeline subjected to transverse PGD (due to landslide or lateral spreading) can be obtained using a formulation similar to the one employed for the strike-slip faults, to be discussed in paragraph 2.6, with the value of crossing angle β equal to zero. This methodology is valid for the case where the size of moving soil mass W, illustrated in Figure 8, is large enough so that it exceeds the length L calculated from equation (#). In the case where the size W of the moving soil mass is comparable to the value of length L, an estimate of bending strain can be obtained with Eq. 3.

$$\varepsilon_b = \pm \frac{\pi D \delta}{W^2} \qquad \text{Eq. 3}$$

- Analysis for Fault Crossing

A continuous pipe will experience plastic deformations in most actual fault crossing situations. Therefore, the pipe must be ductile and resilient and the joints capable of developing the required ground-induced deformation without loss of containment. The average pipe strain may be estimated (in a non-rigorous manner) as follows if the fault offset results in net tension in the pipe:

$$\varepsilon_{pipe} = 2\left[\frac{\delta}{2L_a}\cos\beta + \frac{1}{2}\left(\frac{\delta}{2L_a}\sin\beta\right)^2\right] \qquad \text{Eq. 4}$$

where, β is the acute angle between the pipe run and line of ground rupture, and L_a is the effective unanchored pipe length, defined as the distance between the fault trace and an anchor point, as shown in Figure 9.

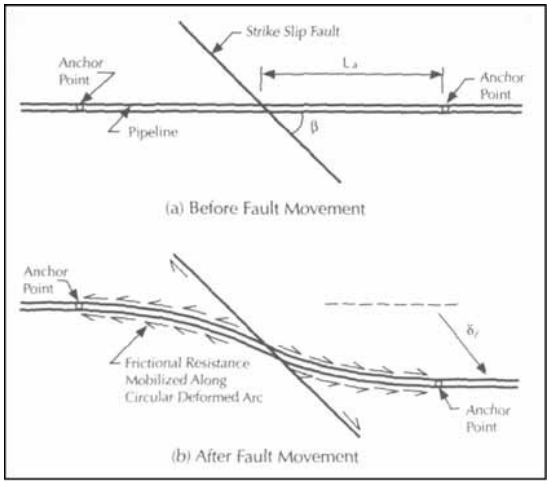

Figure 9. *Plan View of Pipeline*

In the absence of bends, tie-ins or other constraints near the fault, the axial resistance is provided by the soil-pipe friction and the effective unanchored pipe length can be estimated as follows.

$$L_\alpha = \frac{P}{t_u} \qquad \text{Eq. 5}$$

where, P is actual tensile force in the pipe at the fault crossing and t_u is the maximum soil resistance to the pipe axial direction per unit length of pipe. The value of P is not well-defined a priori and its calculation requires an iteration procedure.

2.3 Beam type model for simulation of buried pipelines

As a more rigorous alternative to design analytical equations, it is possible to employ the finite element method to model the effects of ground-induced actions on a buried pipeline. This analysis requires some computational effort and expertise, but offers an advanced tool for determining stresses and strains within the pipeline wall with significantly increased accuracy with respect to the analytical formulae described above. There exist two levels of finite element modeling. The first level is adequate for regular design purposes, whereas the second level, which employs a 3D continuum approach, is used only in special cases, where increased accuracy is necessary. In the following, a short description of the first level approach is offered.

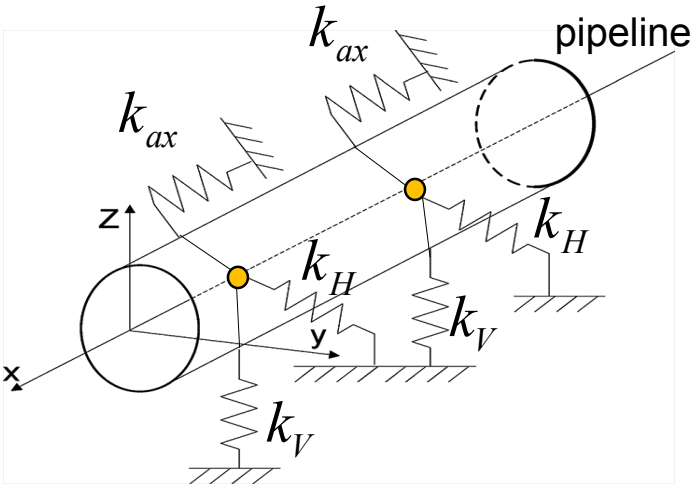

Figure 10. Simplified finite element model; pipe (beam-type) finite elements and soil springs attached to pipeline nodes in the three principal directions.

- Finite element analysis using beam-type elements

In this type of analysis, the pipe is modelled with beam-type one-dimensional finite elements. Both transient and permanent actions on a buried pipeline can be modelled through finite element analysis. Nevertheless, this numerical methodology has been mainly employed for simulating permanent ground-induced actions on pipelines, such as faults, landslides and lateral spreading. The finite element mesh near discontinuities (e.g. fault plane) should be fine enough, so that gradients of stress and strains are accurately simulated.

Type of finite elements: The use of regular beam elements for the pipeline model is not recommended, given the fact that they cannot account for pressure loading. Instead, "pipe elements" are preferable, which account for the presence of hoop stress and strain due to pressure. Furthermore, the use of "pipe elements" with the capability of describing cross-sectional ovalization, sometimes referred to as "elbow elements", can further improve the accuracy of the finite element model, especially at pipe bends. Instead, if the pipe elements assume a circular cross-section throughout the analysis, ovalization effects at pipe bends can be taken into account through appropriate flexibility factors, and stress intensity factors.

Pipe and soil modelling: The finite element model should take into account both material and geometric nonlinearities. The pipe material should be modelled as elastic-plastic, considering also strain hardening effects. Furthermore, the ground surrounding the pipeline should be modelled by appropriate springs (Figure 9), attached on the pipe nodes and directed in the transverse directions (denoted as k_v and k_h for the vertical and lateral direction respectively) and the axial direction (k_{ax}). The nonlinear "law" of the soil springs in all directions should represent the nonlinear load-deformation of the soil, including possible slip of the pipe through the soil. Thus, the load-deflection curves of the soil spring should be nonlinear. Expressions for the axial and the transverse springs are offered in ALA (2001) Guidelines, based on the type of soil. Alternative equations for those springs are offered in NEN 3650 standard. In any case, the design engineer may modify the proposed equations for the springs, if more detailed information on the actual field conditions is available, either from test data, or his engineering judgment.

Analysis procedure and output: To conduct pipeline analysis subjected to permanent ground deformation, appropriate displacements should be applied to the ends of the soil springs. The analysis should be conducted in three consecutive steps: (a) gravity loading, (b) operational loading (pressure and temperature) and (c) application of PGD. The analysis output consists of stress resultants in pipeline cross-sections, as well as the stresses and strains in the longitudinal direction. The user should be cautioned that if the finite elements are not capable of describing accurately cross-sectional distortion these stresses and strains may be quite different than the real stresses and strains in the pipeline wall. These differences are very significant when the pipe wall begins to wrinkle due to local buckling. Consideration of local stresses due to pipe wall wrinkling locations requires a more detailed analysis, with the use of shell elements for modelling the pipe.

2.4 Kennedy et al. (1977) method for fault crossing analysis

An analytical method for estimating stresses and strains in a buried pipeline crossing a fault and subjected to large fault displacements has been proposed by Kennedy et. al. (1977). This analytical methodology enhances the methodology proposed by Newmark and Hall (1975) and is based on the consideration of the pipeline as a cable, ignoring pipeline bending stiffness. Figure 1 shows the pipeline crossing a right lateral fault at an angle β with respect to the direction of movement. The pipe is assumed to be anchored at distance L_1 and L_2 on two far ends. This method is limited to crossing angles that result in pipe elongation a common case in pipeline applications. The steps of this analytical methodology are stated below.

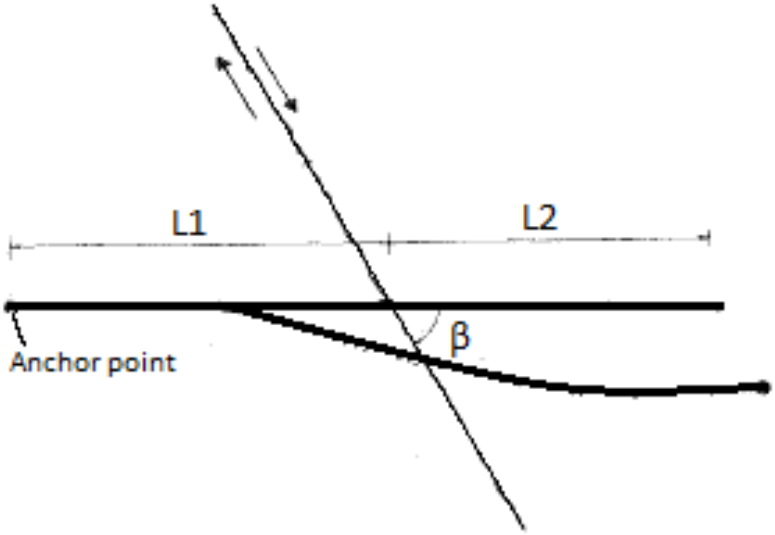

Figure 11. Schematic diagram of Shallow buried pipe movement resulting from horizontal fault displacement.

(a) Estimate maximum axial stress σ_M and force axial F_M in the pipe at fault.

(b) Approximate the lateral and vertical radii of curvature from Eq 6 below, substituting F_M for F_x and p_u and q_u for P_{lx} and P_{ux} respectively. The value of p_u is the maximum soil resistance per unit pipe length in the transverse (horizontal) direction, while q_u is the maximum soil resistance per unit pipe length in the vertical downward direction.

$$R_{cL} = \frac{1}{\kappa_h} = \frac{F_x}{P_{lx}} \quad , \quad R_{cv} = \frac{1}{\kappa_v} = \frac{F_x}{P_{ux}} \qquad \text{Eq. 6}$$

(c) Determine the value of lengths L_{cL}, L_{cv} over which lateral and vertical displacement occurs due to curvature $k_h=1/R_{cL}$ and $k_v=1/R_{cv}$, respectively from Eq. 7 and the total pipe elongation $\Delta L_{required}$ from Eq. 8.

$$L_{cL}=\sqrt{R_{cL}\delta_h \sin\beta} \quad , \quad L_{cv}=\sqrt{2R_{cv}\delta_v} \qquad \text{Eq. 7}$$

$$\Delta L_{required}=\delta_h \cos\beta+\frac{\left(\delta_h \sin\beta\right)^2}{3L_{cL}}+\frac{2\delta_v^2}{3L_{cv}} \qquad \text{Eq. 8}$$

(d) Determine the total elongation $\Delta L_{available}$ of the pipeline as the sum of the elongations in the straight and curved zones from Eq. 9.

$$\Delta L_{available}=\Delta L_{s1}+\Delta L_{s2}+2\Delta L_c \qquad \text{Eq. 9}$$

where the values of ΔL_{s1}, ΔL_{s2}, ΔL_c are calculated from Eq. 10 to Eq. 12 written below.

$$\Delta L_c=\varepsilon_y\left\{L_{cL}\left(\frac{B_M+B_S}{2}\right)+\frac{C}{h_c(r+2)}\left[(B_M)^{r+2}-(B_s)^{r+2}\right]\right\} \qquad \text{Eq. 10}$$

$$\Delta L_{s1}=\varepsilon_y\left\{L_{cL}1\left(\frac{B_{L1}+B_S}{2}\right)+\frac{C}{h_s(r+2)}\left[(B_s)^{r+2}-(B_{L1})^{r+2}\right]\right\} \qquad \text{Eq. 11}$$

$$\Delta L_{s2}=\varepsilon_y\left\{L_{cL2}\left(\frac{B_{L2}+B_S}{2}\right)+\frac{C}{h_s(r+2)}\left[(B_s)^{r+2}-(B_{L2})^{r+2}\right]\right\} \qquad \text{Eq. 12}$$

where

$$L_{cL1}=L_1-L_{cL} \quad , \quad L_{cL2}=L_2-L_{cL} \qquad \text{Eq. 13}$$

$$B_M=\frac{\sigma_M}{\sigma_y} \quad , \quad B_s=B_M-h_c L_{cL} \qquad \text{Eq. 14}$$

$$B_{L1}=B_s-h_s L_{sL1} \quad , \quad B_{L2}=B_s-h_s L_{sL2} \qquad \text{Eq. 15}$$

and

$$h_c=\frac{f_c}{A_p\sigma_y} \quad , \quad h_s=\frac{f_s}{A_p\sigma_y} \qquad \text{Eq. 16}$$

In the above equations, f_s and f_c are the longitudinal friction at straight and curved sections, respectively, f_s is the maximum soil resistance in axial direction per unit length of pipe, while the ratio of curved pipe zone to straight pipe zone friction factors raging from 2.4 for H_c/D equal to 1, to 3.3 for H_c/D equal to 3. Finally A_p is the cross sectional area, σ_y the yield stress of the pipe material whereas and L_1 and L_2 are the estimated unanchored lengths on each side of the fault.

(e) If the value of $\Delta L_{required}$ is not equal to $\Delta L_{available}$ then the initial estimates of axial stress σ_M and force F_M is revised and steps (a)-(d) are repeated until the values of $\Delta L_{required}$ and $\Delta L_{available}$ become equal.

(f) Upon convergence of the method, as described above, the axial strain ε_x are determained from the stress-strain curve of Eq. 17 (Ramberg–Osgood curve).

$$\varepsilon_x = \frac{\sigma_x}{E}\left[1+\left(\frac{a}{r+1}\right)\left(\frac{|\sigma_x|}{\sigma_y}\right)^r\right] \qquad \text{Eq. 17}$$

In the above expressions parameters a, r are the Ramberg-Osgood coefficients for steel pipe material, σ_y is the yield stress of the material, δ_h and δ_v are the fault displacements in the parallel and vertical direction with respect to fault axis, respectively. Due to its complexity and its repetitive form, the application of the above methodology requires a computer programming.

2.5 Vazouras et al. (2012) method for strike-slip faults

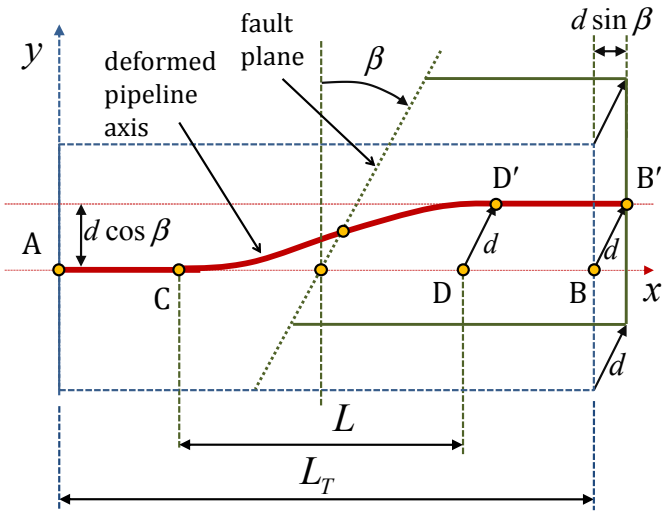

Figure 10. Schematical representation of fault-induced deformation of pipeline axis.

A simplified analytical formulation has been proposed in a series of publications by Vazouras et al. (2010, 2012 and 2015) for describing pipeline deformation under strike-slip fault action, using an assumed-shape function for the deformed shape of the pipeline. The methodology is based on an assumed shape for the transverse pipeline deformation in an S-shaped "shearing type" configuration, within a segment of length L, as shown in Figure 10 the pipeline outside this segment of length L is assumed to be under pure tension only. A shape function for the transverse displacement u(x) of the pipeline is considered in the following form:

$$u(x) = \frac{d}{2}\cos\beta\left(1-\cos\frac{\pi x}{L}\right) \qquad \text{Eq. 18}$$

where x=0 and x=L are the two ends of the S-shape pipe segment. In addition, the axial displacement v(x) of the pipeline within this segment due to longitudinal stretching is assumed to be linearly distributed along the pipeline:

$$v(x) = \frac{d\sin\beta}{L}x \qquad \text{Eq. 19}$$

In Eq. 18 and Eq. 19 the d is the fault displacement, β and L is the crossing angle and the length of S-shape as shown in Figure 10, respectively. Having estimated the maximum bending curvature, k, due to the imposed deformation d and neglecting cross-sectional distortion, the corresponding bending stain ε_b is

$$\varepsilon_b = \frac{kD}{2} = \frac{\pi^2}{4}\left(\frac{d\cos\beta}{L}\right)\left(\frac{D}{L}\right) \qquad \text{Eq. 20}$$

while the axial membrane strain ε_m can be computed from Eq. 21 equation reference goes here, where the first term is due to axial stretching due to bending and the second term is due to elongation due to the fault displacement component in the direction of pipeline axis.

$$\varepsilon_m = \left(\frac{d^2\pi^2\cos^2\beta}{16L^2} + \frac{d\sin\beta}{L}\right)\left(\frac{\omega}{\omega+1}\right) \qquad \text{Eq. 21}$$

where the parameters ω, λ and $\overline{K}_t$ are given from Eq. 22, Eq. 23 and Eq. 24, respectively.

$$\omega = \frac{\overline{\mathrm{K}}_t L}{2E_s A} \qquad \text{Eq. 22}$$

$$\lambda = \sqrt{\frac{\pi D k_s}{E_s A}} \qquad \text{Eq. 23}$$

$$\overline{K}_s = \lambda \mathrm{E}_s A \qquad \text{Eq. 24}$$

In the above equations, E_s is the Young's modulus of steel pipe material and A is the cross sectional area of the pipe. Furthermore, parameter k_s is given from Eq. 25 where the t_u is the maximum soil resistance per pipe unit length in the pipe axial direction.

$$k_s = \frac{t_u}{\pi D} \qquad \text{Eq. 25}$$

An important parameter for this methodology is the length L of the S-shape of the pipeline. A formulation for the prediction of this length is presented in the following paragraph 2.6, while a comparison of this method with finite elements is presented in paragraph 2.7.

2.6 New methodology for analyzing fault crossing cases

As descripted in the previous paragraph Vazouras et. al (2010, 2012 and 2015) proposed a simplified method for analyzing pipelines which crosses strike-slip faults. An important missing parameter of this methodology is the length L of the deformed S-shape of the pipeline as shown in Figure 10. In Figure 11 an equivalent static model for the calculation of the length L of deformed S-shape of the pipeline is shown. The moment diagram (a) is the result of the support movement while the moment diagram (b) is the result of the distributed loading. The fault movement induces a moment in the length L, which can be described by the moment diagram (c) of Figure 11.

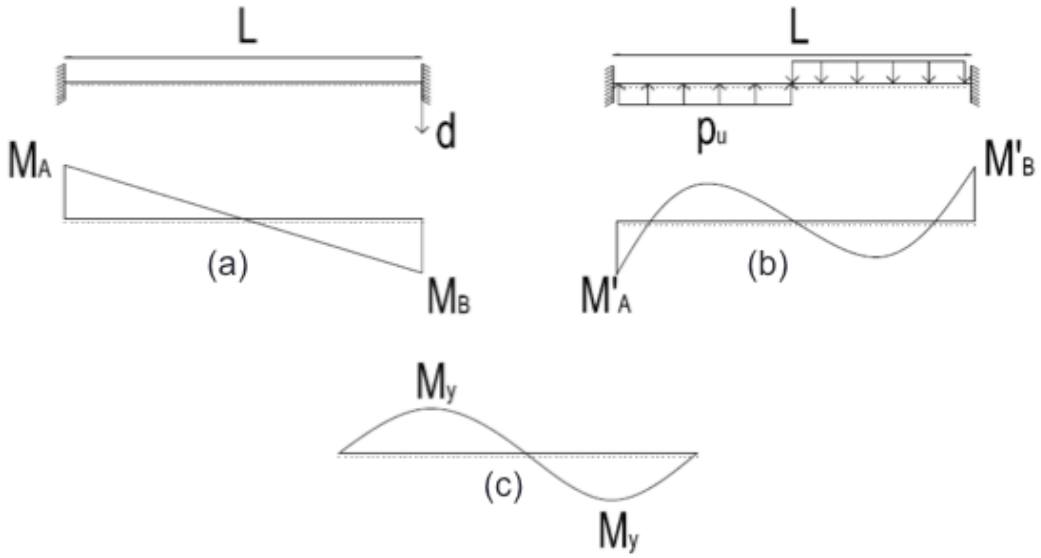

Figure 11. Equivalent static model for the calculation of the length L of the deformed S-shape of the pipeline in a case of a strike-slipe fault.

The elastic beam theory is employed in order to calculate the length L of the deformed shape of pipeline. In particular, the two loading conditions of Figure 11, are combined in order to simulate the loading conditions of the pipe due to fault movement. The support movement is employed in order to take account the fault displacement while the distributed loading in order to take account of the soil resistance p_u (maximum soil resistance to the pipe transverse direction per unit length of the pipe). The length L results by solving the system of Eq. 26 and Eq. 27. The

solution of the system of Eq. 26 and Eq. 27 gives the length L at which the combination of loadings of Figure 11 gives zero moment in the supports and yield moment of the pipe cross section intermediate of the deformed length of the pipe. According to this procedure the length L is given by Eq. 28 where the M_y is the yield moment of the pipe cross section and p_u is the maximum soil resistance to the pipe transverse direction per unit length of the pipe.

$$M_A + M'_A = 0 \Rightarrow 0.03125 L^4 p_u - 6dEJ = 0 \qquad \text{Eq. 26}$$

$$0.01562 L^4 p_u - M_y L^2 + 3EJd = 0 \qquad \text{Eq. 27}$$

$$L = \frac{29}{5}\sqrt{\frac{M_y}{p_u}} \qquad \text{Eq. 28}$$

In the above equations the E is the Young's Modulus, J the inertia moment of the pipe cross section while d is the fault displacement. The length L of the deformed S-shape of the pipe from Eq. 28 can be used directly in Vazouras et. al methodology which is described in the previous paragraph.

This methodology is applicable only for strike-slip faults, otherwise in a case of normal or oblique faults some alterations must be done. The maximum soil resistance in the vertical direction is different for the downwards and the upwards direction. This difference is taken into account through some alteration in the equivalent static model as shown in Figure 12.

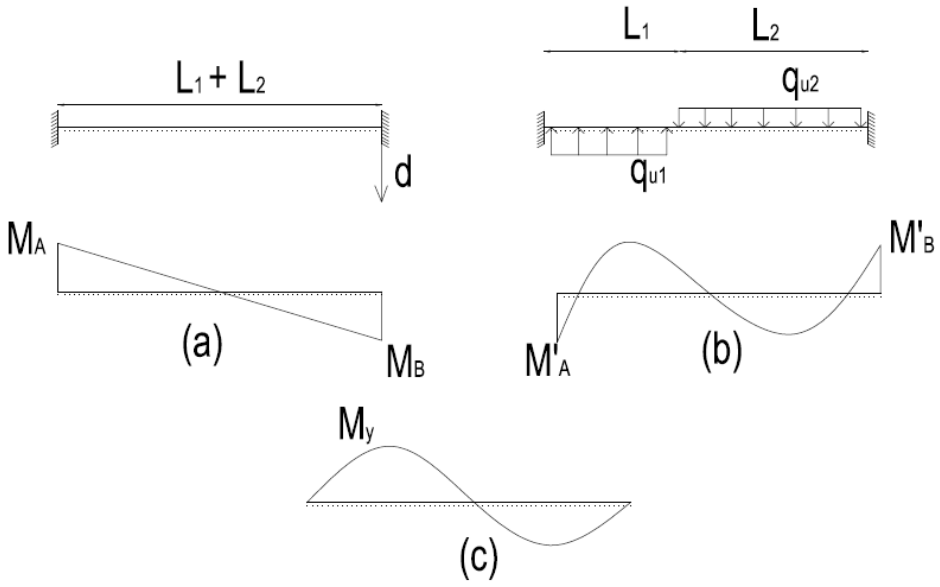

Figure 12. Equivalent static model for the calculation of lengths L_1 and L_2 of the deformed S-shape of the pipeline in a case of normal or oblique fault.

The reaction moments of diagram (b) of Figure 12 can be computed from Eq. 29 to Eq. 31 and the vertical reaction of support (A) V_A can be computed by Eq. 32. The reaction moment of diagram (a) can be computed by Eq. 33. The solution of the system of Eq. 34 and Eq. 35 gives the lengths L_1 and L_2 at which the combination of loadings of Figure 12 gives zero moment in the supports for different values of d. A simplified way to solve this problem is to use the Eq. 36 which is the difference between Eq. 34 and Eq. 35.

$$\gamma_1 = \frac{L_1}{L_1 + L_2} \qquad \gamma_2 = \frac{L_2}{L_1 + L_2} \qquad \text{Eq. 29}$$

$$l_1 = -\frac{1}{3} q_{u1} L_1^2 \gamma_1 (1 - 0.75\gamma_1) \qquad l_2 = -\frac{1}{3} q_{u2} L_2^2 \gamma_2 (1 - 0.75\gamma_2) \qquad \text{Eq. 30}$$

$$M'_A = \frac{1}{3}\left[r_1 + l_2 - 2l_1 - 2r_2\right] \qquad M'_B = \frac{1}{3}\left[r_2 + l_1 - 2l_2 - 2r_1\right] \qquad \text{Eq. 31}$$

$$V_A = \frac{1}{L_1 + L_2}\left(M'_A - M'_B - q_{u1}\frac{L_1^2}{2} + q_{u2} L_2 \left(L_1 + \frac{L_2}{2} \right) \right) \qquad \text{Eq. 32}$$

$$\mathrm{M_A} = -\frac{6EJd}{(L_1 + L_2)^2} \qquad \mathrm{M}_B = \frac{6EJd}{(L_1 + L_2)^2} \qquad \text{Eq. 33}$$

$$\mathrm{M_A} + \mathrm{M'_A} = 0 \Rightarrow$$

$$27.8 L_1^4 q_{u1} + 111 L_1^3 L_2 q_{u1} + L_1^2 L_2^2 (-167 q_{u1} + 333 q_{u2}) + 111 L_1 L_2^3 q_{u2} + 27.8 L_2^4 q_{u2} = 6000 dEJ$$

Eq. 34

$$\mathrm{M_B} + \mathrm{M'_B} = 0 \Rightarrow$$

$$27.8 L_1^4 q_{u1} + 111 L_1^3 L_2 q_{u1} + L_1^2 L_2^2 (-167 q_{u2} + 333 q_{u1}) + 111 L_1 L_2^3 q_{u2} + 27.8 L_2^4 q_{u2} = -6000 dEJ$$

Eq. 35

$$L_1 = \frac{1}{L_2}\sqrt{\frac{24EJd}{(q_{u1} - q_{u2})}} \qquad \text{Eq. 36}$$

$$M_y = M'_A + \frac{V_A^2}{q_{u1}} + \frac{2M_A}{L_1 + L_2}\left(\frac{L_1 + L_2}{2} - \frac{V_A}{q_{u1}} \right) \qquad \text{Eq. 37}$$

The desired set of L_1, L_2 and d is the one that verifies the Eq. 37 which concerns the maximum moment of diagram (c) of Figure 12. The steps of this analytical methodology are stated below.

(a) Calculation of L_1 using Eq. 34 and Eq. 36 for different values of d.

(b) Calculation of L_2 using Eq. 35 for different values of d.

(c) Check which set of L_1, L_2 and d verifies the Eq. 37.

In order to calculate the strains in a case of normal or oblique faults the methodology of Vazouras et. al can be used on the condition of a slight change of the initial assumed shape of the deformed pipe. The axial displacement v(x) of the pipeline within this segment due to longitudinal stretching, which is assumed to be linearly distributed along the pipeline, remains the same, while the shape function for the transverse displacement u(x) of the pipeline is considered only for the part with the larger soil resistance q_u. This assumption is based on the fact that the maximum moment occurs within the segment with the larger soil resistance. The shape function and therefore the maximum bending strain will be computed for a segment with length equal to $2L_i$, where i is the part with the larger soil resistance.

$$u(x) = \frac{d}{2}\cos\beta\left(1 - \cos\frac{\pi x}{2L_i}\right), 0 \le x \le L_i \qquad \text{Eq. 38}$$

$$v(x) = \frac{d\sin\beta}{L_1 + L_2}x \qquad \text{Eq. 39}$$

According to the above alterations the Eq. 20, Eq. 21 and Eq. 22 are changed to Eq. 40, Eq. 41 and Eq.42, respectively.

$$\varepsilon_b = \frac{\pi^2}{4}\left(\frac{d\cos\beta}{2L_i}\right)\left(\frac{D}{2L_i}\right) \qquad \text{Eq. 40}$$

$$\varepsilon_m = \left(\frac{d^2\pi^2\cos^2\beta}{16(L_1 + L_2)^2} + \frac{d\sin\beta}{L_1 + L_2}\right)\left(\frac{\omega}{\omega + 1}\right) \qquad \text{Eq. 41}$$

$$\omega = \frac{\bar{K}_t(L_1 + L_2)}{2E_s A} \qquad \text{Eq. 42}$$

2.7 Comparison between simplified finite element model and analytical methodologies

Two case studies have been analyzed in the coarse of the present work in order to compare the above methodologies. Case study (a) compares the design equations according ALA (2001) for longitudinal soil displacement due to liquefaction with the simplified finite element model while the case study (b) compares the analytical methodology for strike-slip faults with the simplified finite element model.

A 42-inch-diameter, X60 steel pipeline with 0.562-inch thickness is considered in a geohazard area, with cohesionless soil conditions. A comparison between design equations and finite element analysis with beam-type pipe elements is offered in the present paragraph. Soil properties of the cohesionless (sand) soil, geometric parameters and the material of the pipe are presented in Table 1. The loading patterns under consideration are (a) longitudinal PGD due to liquefaction and (b) strike-slip fault crossing.

Table 3. Soil parameters and geometric/mechanical properties.

φ	34^{O}
K_O	0.5
γ (kg/m^3)	1760
H_c (m)	0.9
D (in)	42
t (in)	0.562
Material	X60

(a) Longitudinal PGD due to liquefaction

In this case, the length of liquefied zone L_s (Figure 7) is assumed 100 m (from geotechnical investigation) and the displacement of moving soil mass δ is taken equal to 3 m. For the finite element analysis, pipe elements are adopted and the corresponding results indicate a value for the maximum axial stress equal to **24.7 MPa**. The distribution of axial stresses along the pipeline axis is presented in Figure 13. The computed maximum stress based on the analytical design Eq. 1 and Eq. 2 is **24.1 MPa**. The results obtained from the finite element analysis and the analytical design equations are in very good agreement.

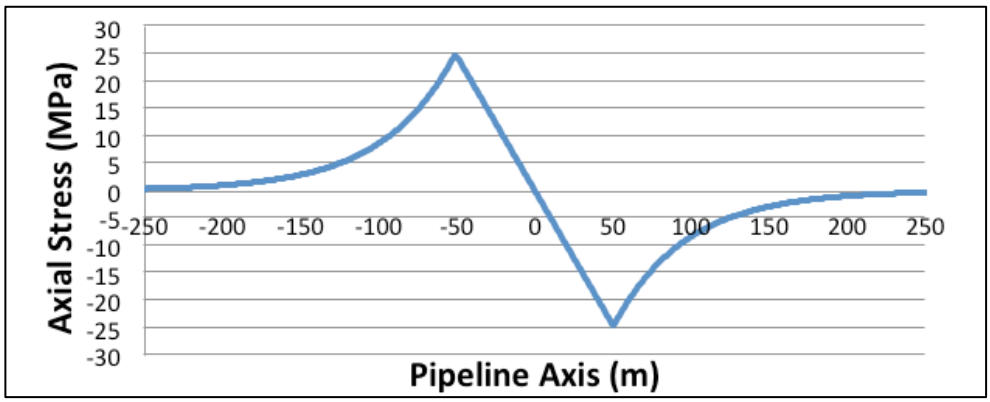

Figure 13. Axial stresses with respect to pipeline axis.

(b) Fault crossing analysis

In this case a strike-slip fault has been considered with two different fault crossing angles β, namely 0^o and 10^o degrees. The analysis is performed for fault displacement equal to 1, 2 and 3 meters for each angle β. The results from the finite element analysis and the results from the analytical design equations of the methodology presented by Vazouras et al. (2015) are presented in Tables 2 and 3 for the two values of crossing angle β, 0^o and 10^o degrees, respectively. The length L of the curved pipe segment is computed from Eq. 28 equal to 28.42 m and the comparison with the deformed shape of the pipe from FE analysis is depicted to Figure 14. The comparison of maximum axial strains and length L between FE analysis and design equations indicates a fairly good agreement.

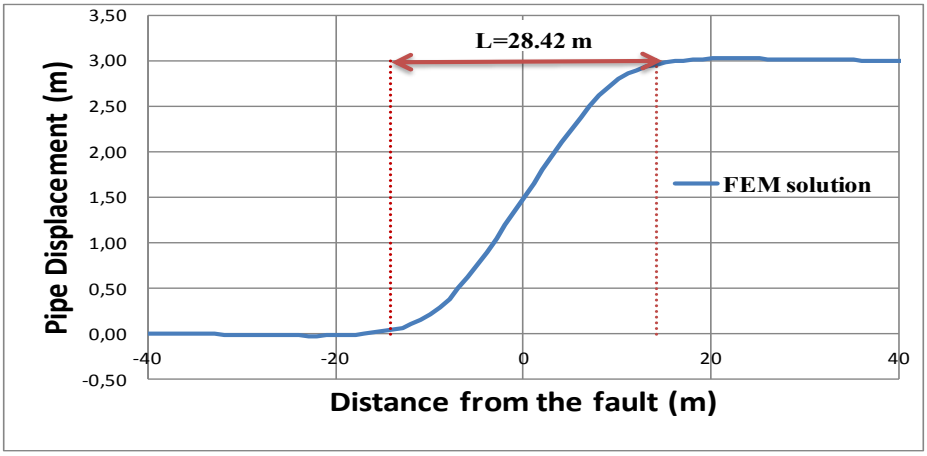

Figure 14. Comparison between length L from equation 1 with the deformed shape of pipeline from FE analysis with pipe elements.

Table 4. Comparison between Design Equation and FEM results for angle β equal to 0^o.

	Max tensile strain %		**Max compressive strain %**	
δ (m)	Design Eq.	FEM	Design Eq.	FEM
1	0.35	0.34	0.31	0.26
2	0.73	0.94	0.59	0.67
3	1.15	1.24	0.83	0.73

Table 5. Comparison between Design Equation and FEM results for angle β equal to 10^o.

	Max tensile strain %		**Max compressive strain %**	
δ (m)	Design Eq.	FEM	Design Eq.	FEM
1	0.48	0.44	0.16	0.18
2	1.00	1.01	0.29	0.26
3	1.56	1.31	0.39	0.24

3. Pipe-Soil Interaction

3.1 Introduction

In the framework of a European Research project, the GIPIPE project, a series of tests had been performed by CSM, in Sardinia, with the aim at examining experimentally soil-pipeline interaction under ground-induced actions. In particular, three pull-out and three transversal tests conducted in order to verify the pipe soil interaction in the axial and the transversal direction, respectively. Moreover four full-scale landslide/fault tests have been performed in order to investigate the complex pipe soil interaction in a realistic scenario. In Table 6, the details on the experimental testing parameters are illustrated for axial, transversal and landslide tests. In all cases, the diameter of pipe specimens is equal to 219.6 mm, the wall thickness is equal to 5.56 mm and the steel grade is API5L X65.

Table 6. Information about experimental testing conducted by CSM.

Test	Compaction Level D_r (%)	Mass density (Kg/m^3)	Water content (%)	Coating	Internal pressure (MPa)
Axial 1	40	1629	5.7	Bare	0
Axial 2	20	1602	7.8	Bare	0
Axial 3	40	1613	5.8	Coated	0
Transversal 1	20	1601	7.6	Bare	0
Transversal 2	40	1640	6.1	Bare	0
Transversal 3	40	1645	7.3	Coated	0
Landslide 1	40	1600	8.0	Bare	0
Landslide 2	40	1688	-	Bare	11.4
Landslide 3	20	1600	-	Bare	0
Landslide 4	20	1600	-	Bare	11.4

In order to define the material parameters for the soil surrounding the pipeline, NTUA performed direct shear tests in samples of sand provided by CSM. In Figures 15 and 16 the variation of internal angle of friction of sand with respect to horizontal

displacement is illustrated for compaction level equal to 20 and 40 %, respectively as obtained by the above tests.

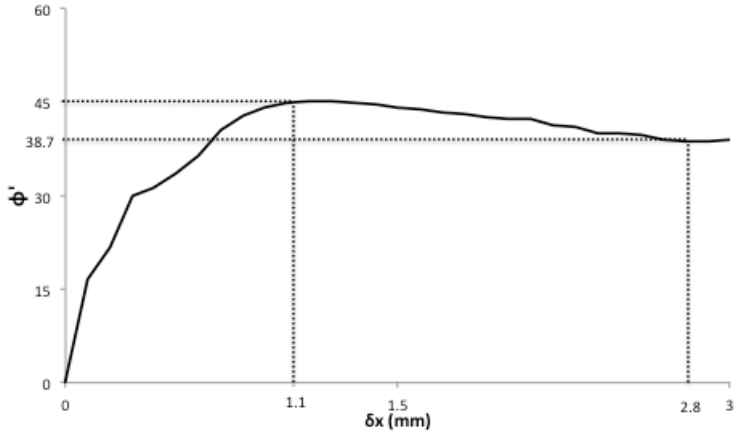

Figure 15. Variation of internal friction angle with respect to horizontal displacement for a sand with D_r = 40 %, based on results from direct shear test conducted by NTUA for vertical applied stress equal to σ_v=17 kPa.

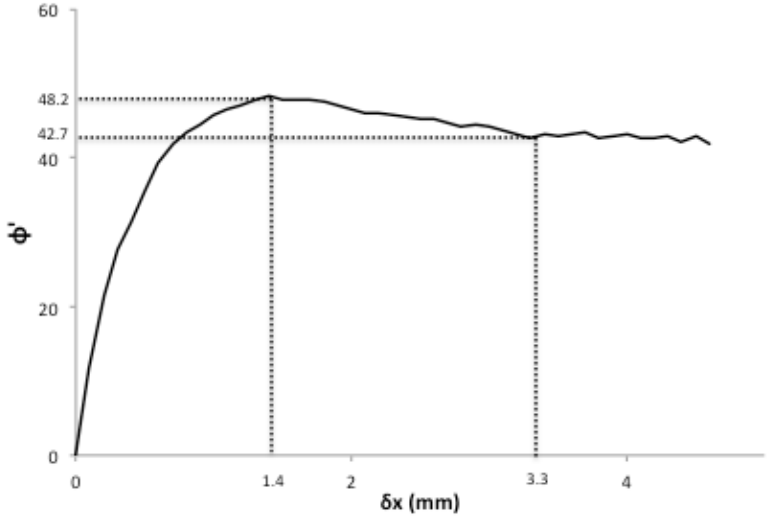

Figure 16. Variation of internal friction angle with respect to horizontal displacement for a sand with D_r = 20 %, based on results from direct shear test conducted by NTUA for vertical applied stress equal to σ_v=17 kPa.

A finite element model has also been developed in order to simulate the experimental testing conducted by CSM. In this model four-node reduced integration shell elements (type S4R) are employed for modeling the cylindrical pipeline segment and eight-node reduced-integration "brick" elements (C3D8R) are employed to simulate the surrounding soil. The mechanical behavior of soil material is described through a modified Mohr-Coulomb model (Anastasopoulos et. al. 2007) in order to account for the softening behavior of the sand.

3.2 Transverse Pipe-Soil Interaction

Pipe-soil interaction in the transverse direction of a buried pipeline is a significant parameter for the deformation of the pipe in the case of permanent ground deformations. Several transverse tests have been performed e.g. (O'Rourke et. al. (1985) and Karimian (2006)) in order to understand and quantify the transverse pipe-soil interaction mechanism. Three new transverse tests have been conducted by CSM in the course of the GIPIPE project. The experimental setup is illustrated in Figures 17 and 18. In those tests the pipe has been restricted in the vertical direction.

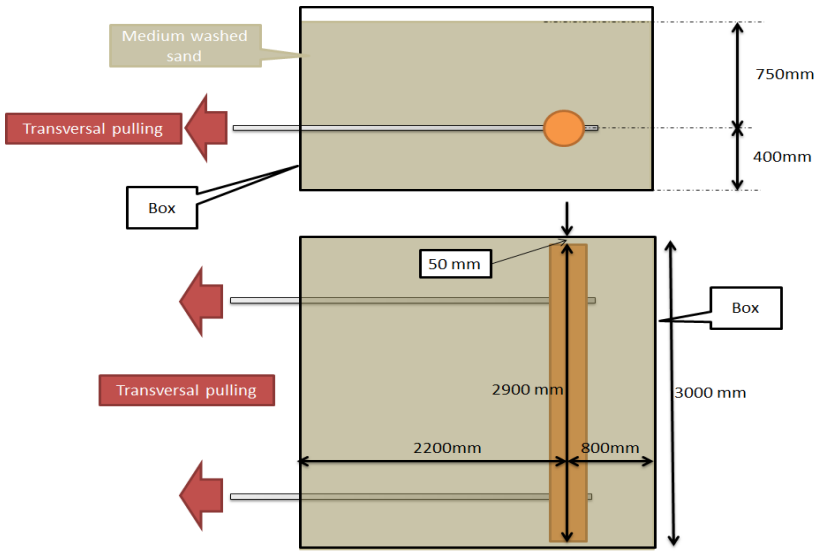

Figure 17. Experimental setup of transverse tests conducted by CSM.

Figure 18. Deformed shape of the soil free surface at the end of the test.

The results of the three tests are shown in Figure 19 in terms of the load displacement diagram. The value of force is calculated from the measurements of the contact pressure sensor wrapper around the pipe, the contact pressure sensor is shown in Figure 20. In general, it is observed that all three tests indicate a similar response, especially for displacement values larger than 400 mm. The small difference of the compaction level between test 1 (Dr = 22%) and tests 2 and 3 (Dr =35%) is reflected to a small difference in the contact pressure for displacements lower than 200 mm.

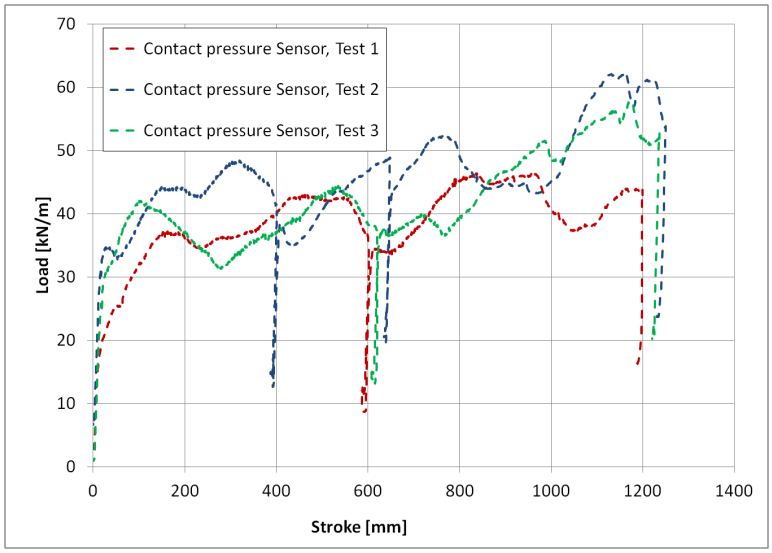

Figure 19. Pressure-sensor force versus stroke for the three transverse tests conducted by CSM.

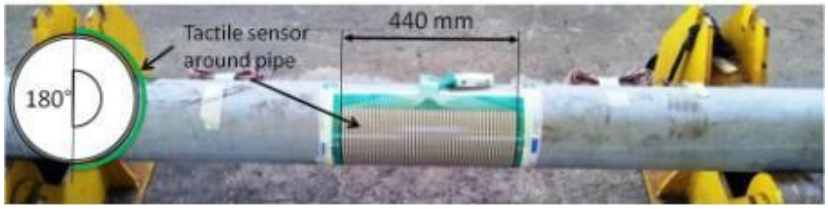

Figure 20. Pressure-sensor wrapper around the pipe.

A finite element model has been developed, which simulates the transverse tests. The model is shown in Figure 21 and 22. In order to reduce the computational effort only a slice of width 0.1m is modeled; this width corresponds to 1 element. The analysis proceeds moving the pipeline in the direction of x axis, as shown in Figure 22, while the displacements in direction of z axis are restricted. A comparison between experimental results and the finite element model described above as shown in Figures 23, 24 for transverse tests 1, 2 and 3, respectively. The predictions of pipe-soil interaction obtained from the finite element model seems to be quite satisfactory.

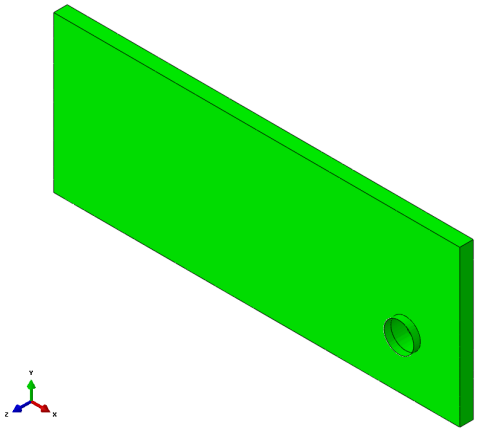

Figure 21. General configuration (solid model) of the CSM transverse test simulation.

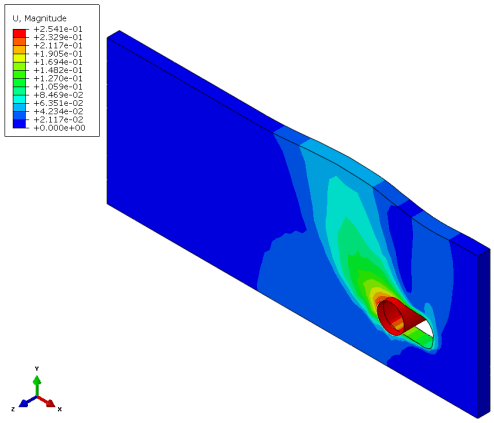

Figure 22. Deformed shape of the finite element model of transverse test corresponding to a value of pipe displacement equal to 250 mm (1.14 pipe diameters).

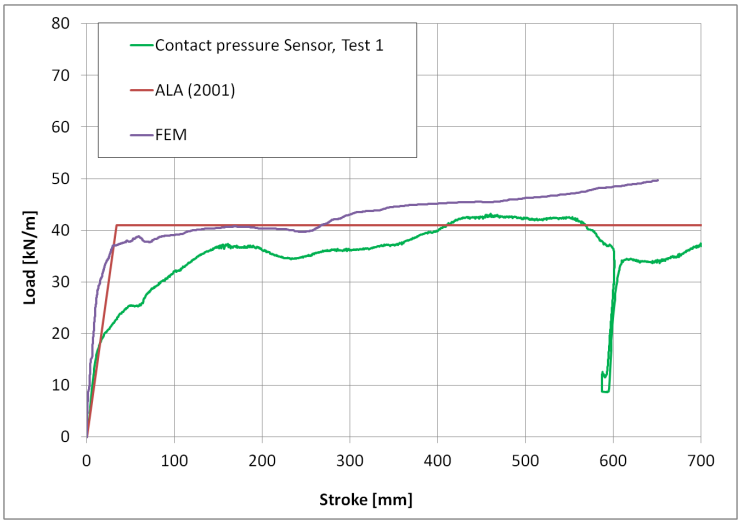

Figure 23. Comparison between Transverse Test 1 results and the results of finite element model.

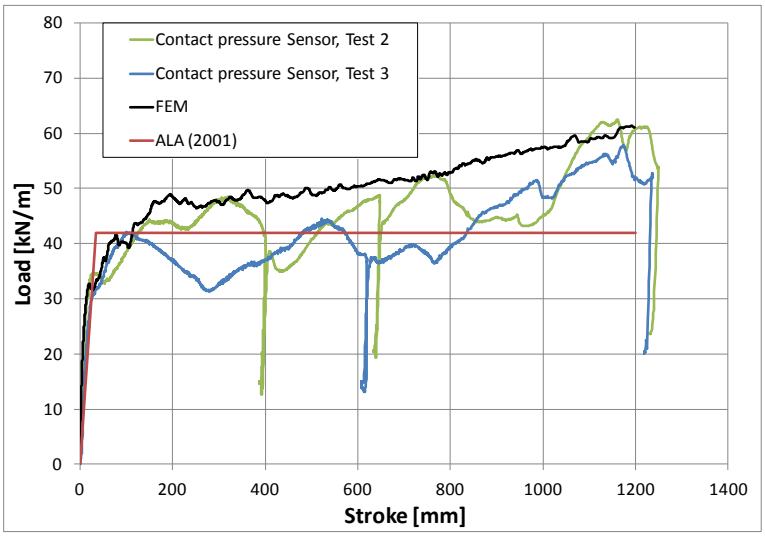

Figure 24. Comparison between Transverse Test 2 and 3 results and the results of the finite element model.

3.3 Axial Pipe-Soil interaction

The pipe-soil interaction in the axial direction may be important for the deformation of the pipe in the case of permanent ground deformations, as well as in the case of seismic wave loading. Several pull out tests have been performed elsewhere, and reported in the previous publications (Scarpelli et. al. (2003), Karimian (2006)) during the last years, in order to determine the axial pipe-soil interaction mechanism. Three new pull out tests have been conducted by CSM in the course of the GIPIPE project. The experimental setup is illustrated in Figure 25 and 26. The results of the three tests are presented briefly in the following Figure 27. The three tests show similarities with the results of a direct shear tests performed on sand samples by NTUA to evaluate the soil friction angle. In both cases, a peak shear resistance is observed, followed by a decay of resistance value towards an asymptotic residual value.

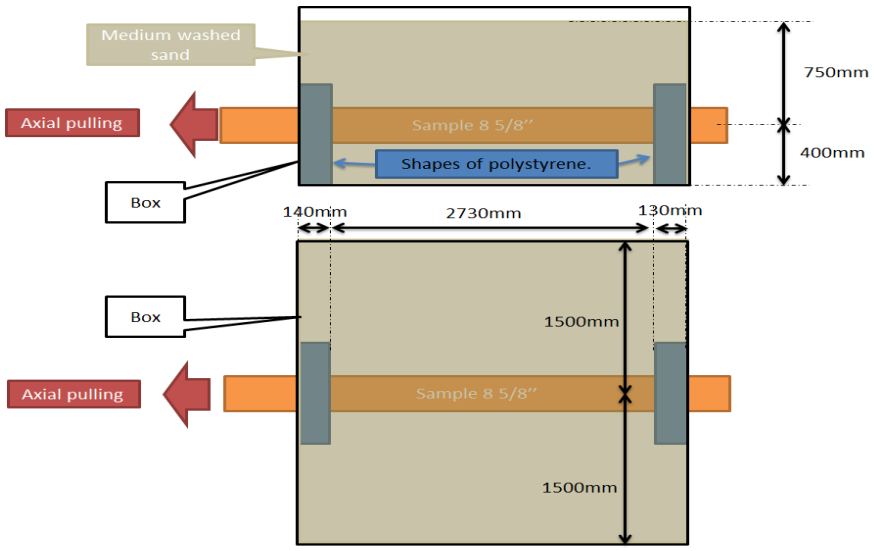

Figure 25. Experimental setup of axial tests conducted by CSM.

Figure 26. Setup of the pull-out tests before at the beginning of testing.

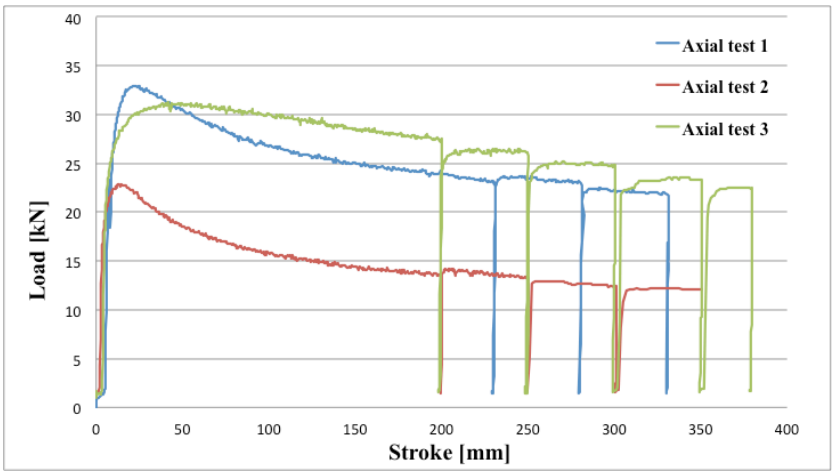

Figure 27. Pull-out load versus stroke for the three axial tests conducted by CSM.

The maximum soil resistance t_u against pipe movement in the axial direction (t_u is force per unit pipe length) according to ASCE guidelines (1984) and ALA guidelines (2001) can be calculated from Eq. 43:

$$t_u = \pi D\left(\frac{\sigma_v + \sigma_h}{2}\right)\tan\delta\varphi \qquad \text{Eq. 43}$$

where the σ_v and σ_h the vertical and the lateral pressure in pipe depth, respectively, φ is the internal friction angle of sand and δ is the pipe-soil interface coefficient. Eq. 43 describes a classical Coulomb friction law. The friction coefficient μ is constant and equal to $\tan\delta\varphi$ while the normal force to the interface is equal to the perimeter of the pipe, multiplied by the average of vertical and lateral earth pressure as shown in following Figure 28.

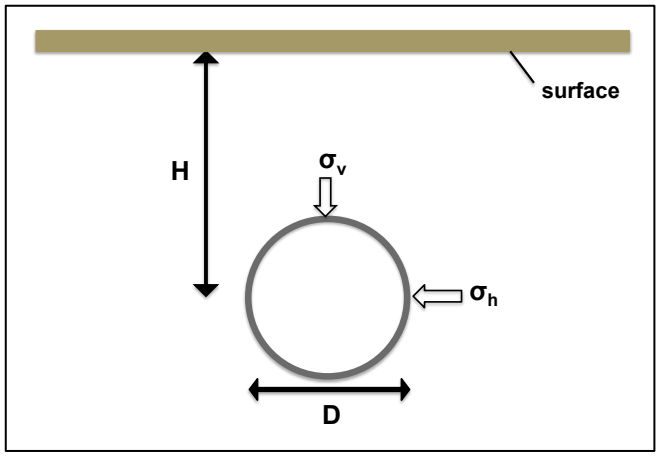

Figure 28. Vertical and lateral earth pressure in the pipe cross section.

In the case of a soil without dilatancy, Eq.43 can describe pipe-soil interaction in the axial direction with very good accuracy. On the other hand, in the case of a soil with dilatancy, Eq. 43 cannot describe satisfactory the pipe-soil interaction. These two cases are analyzed below.

- *Soil without dilatancy*

Karimian et. al. (2006) performed several pull out tests, one test was with sand without dilatancy. The experimental setup is illustrated in Figure 29. The outer diameter of the steel pipe was equal to 457 mm while pipe thickness was 12.7 mm. This test was performed with the embedment of loose sand with a compaction level (D_r) of approximately 20% and an average density equal to 1450 kg/m^3. The depth to

diameter H/D ratio for this test was equal to 2.7, and the length of the soil box equal to 3.8 m. The comparison between experiment, the provisions of ASCE guidelines (1984) and the finite element analysis is presented in Figure 31. In that figure, the axial soil resistance is shown in terms of pipe displacement. The F'_A is the normalized value of axial force, with respect to the vertical effective stress from soil overburden at the centerline of the pipe as calculated from Eq. 44. The model simulates the axial test (pull out test) conducted by UBC (Karimian, 2006) is shown in Figure 30. The pipeline is pulled outwards at the near end, whereas the far end of the pipe remains free. The prediction of axial soil resistance for both ASCE guidelines (Eq. 43) and the finite element analysis is very satisfactory.

$$F'_A = \frac{F}{\gamma' H \pi D L} \qquad \text{Eq. 44}$$

Figure 29. Experimental setup of axial test performed by Karimian (2006).

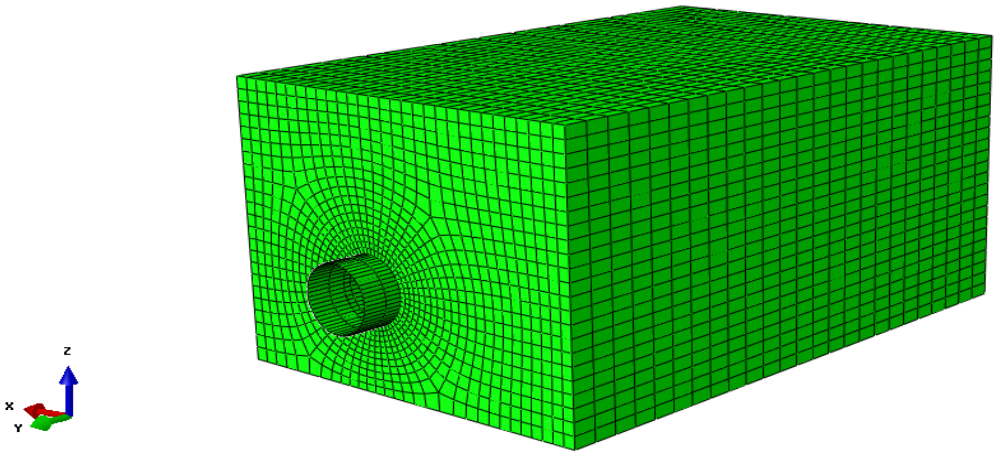

Figure 30. Finite Element Model used for simulating the pull-out test of CSM and the one conducted by Karimian (2006).

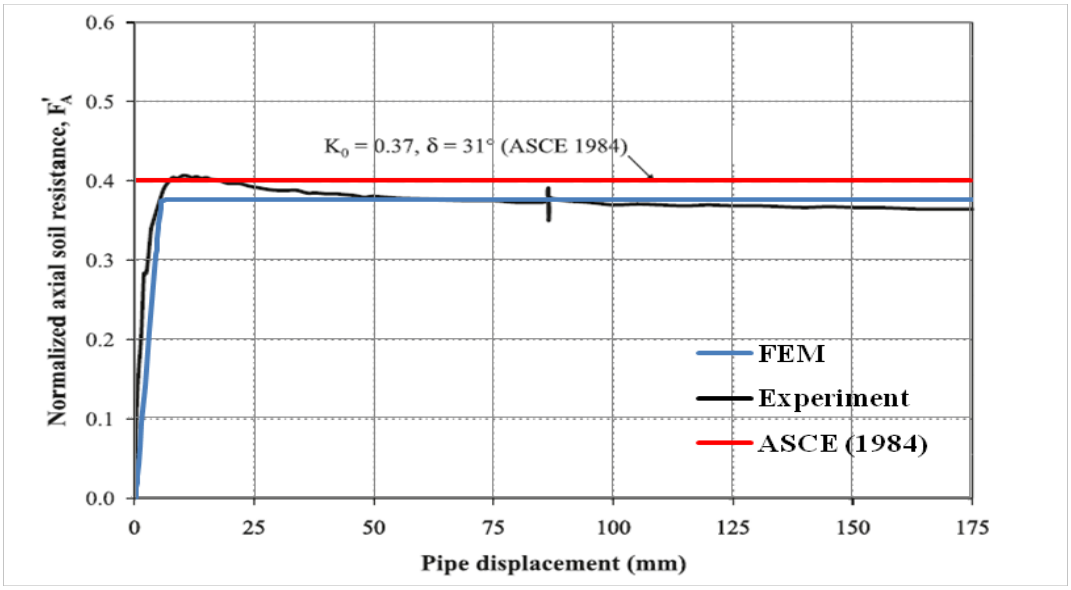

Figure 31. Comparison between the experimental data, the ASCE guidelines (1984) and the results from the finite element analysis.

- *Soil with dilatancy*

In the case of a sand with dilatancy, Eq. 43 cannot predict satisfactory the pipe-soil interaction in axial direction. It is obvious from Figure 32 and from other experiments available in the literature as reported by Scarpelli et. al (2003) and by Karimian (2006)) that the friction in the interface of pipe and sand cannot be descripted adequately by a Coulomb friction. In Figure 32 a comparison between Axial Test 1 conducted by CSM and the provision of ASCE (1984) is depicted for sand with

dilatancy. The prediction of ASCE guidelines is significantly lower than experimental results. This difference is attributed to the fact that the Eq. 43 does not take into account the dilatancy of the sand.

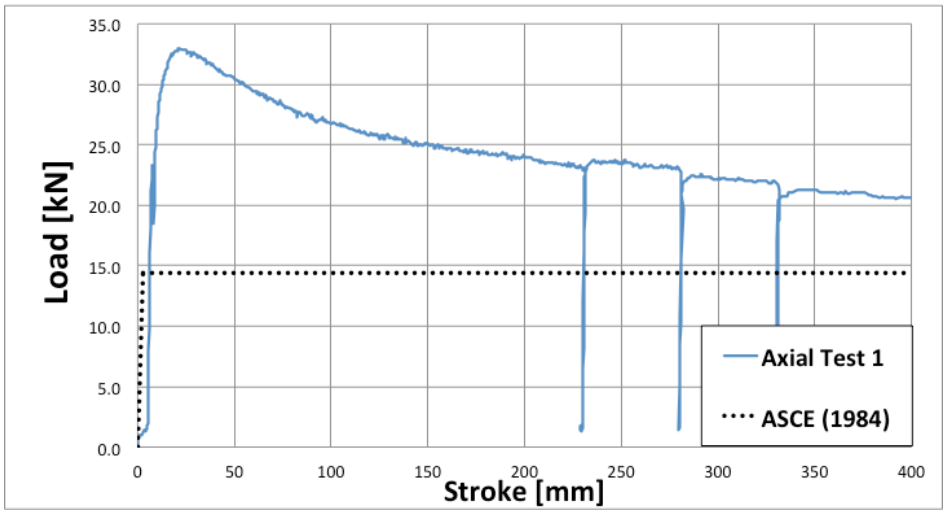

Figure 32. Comparison of axial soil resistance between the experimental results of Axial Test 1 conducted by CSM and the provision of ASCE guidelines (1984).

A schematic representation of shear zone around the pipe caused by axial differential movement between the pipe and the soil is presented in Figure 33. As plastic shear deformation develops in the sand around the pipe, an extra stress Δσ also develops at the pipe-soil interface. This stress Δσ is caused by the fact that the sand under confined shear conditions cannot expand freely.

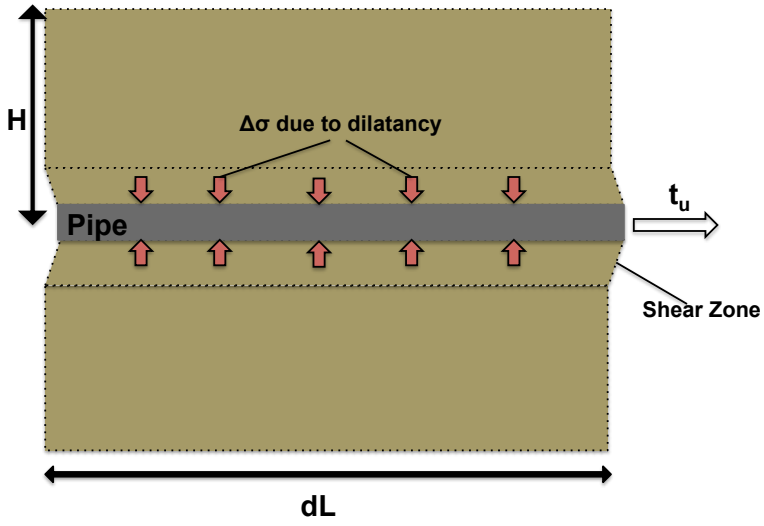

Figure 33. Schematic representation of shear zone around the pipe caused by axial differential movement between pipe and soil (vertical section).

Equations (3) describe a modified law for pipe-soil interaction in the axial direction. An exponential decay law has been introduced to describe the friction coefficient as decreasing function of the relative displacement d between the soil and the pipe μ(d), as well as the extra stress due to sand dilatancy Δσ(d).

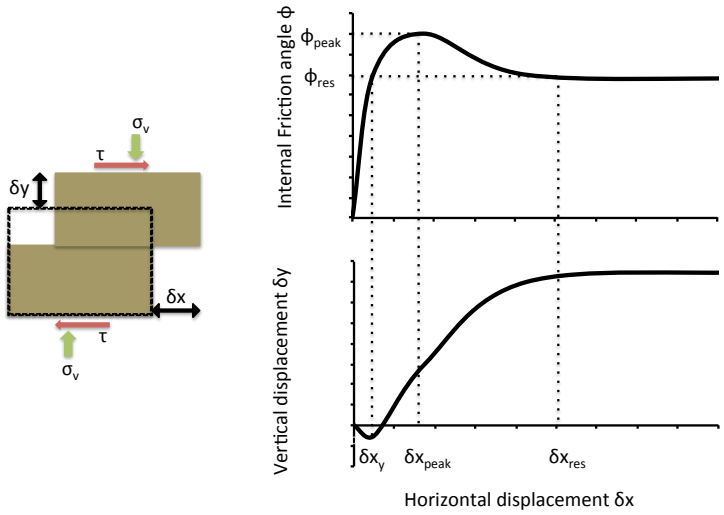

Figure 34. Typical variation of internal friction angle φ and vertical displacement δy with respect to horizontal displacement δx in a direct shear test.

$$t_u(d') = \begin{cases} \pi D\left[\frac{\sigma_v+\sigma_h}{2}+\Delta\sigma_{peak}\right]\tan(\delta\varphi_{peak}), d'=0 \\ \pi D\left[\frac{\sigma_v+\sigma_h}{2}+\Delta\sigma(d')\right]\mu(d'), d'>d_{crit} \end{cases} \quad \text{Eq. 45}$$

In Eq. 45 Δσ(d) and μ(d) are given by Eq.46 and Eq.47, where d_{crit} is the maximum displacement at which maximum soil resistance occurs. According to ALA guidelines (2001) d_{crit} is equal to 0.1 – 0.2 inch for dense to loose sand and d' is the difference between d and d_{crit}, $(d' = d - d_{crit})$.

$$\Delta\sigma(d') = (\Delta\sigma_{res} - (\Delta\sigma_{res} - \Delta\sigma_{peak})e^{-ad'} \quad \text{Eq. 46}$$

$$\mu(d') = (\tan\delta\varphi_{res} - (\tan\delta\varphi_{res} - \tan\delta\varphi_{peak})e^{-ad'} \quad \text{Eq. 47}$$

In Eq. 47, φ_{peak} and φ_{res} are the peak and constant volume internal angle of friction of the sand, respectively (Figure 34) and constant α is given by the empirical Eq. 48. The value of α controls the decay law of the friction coefficient.

$$a = \frac{1}{f(\delta_x - \delta_{xpeak})}\ln\frac{\varphi-\varphi_{res}}{\varphi_{peak}-\varphi_{res}} \quad \text{Eq. 48}$$

In Eq. 48, φ is a random value of internal friction between φ_{peak} and φ_{res} and δx the corresponding horizontal displacement. Eq. 48 describes the rate of decay of internal friction with respect to the horizontal displacement at the direct shear test divided by a factor f, due to the difference of the shear zone width between the direct shear test and the actual problem. Factor f is taken equal to 100 or more for a small diameter pipe while can be equal to 1 for very large diameters, a methodology for the calculation of the factor f is still under investigation.

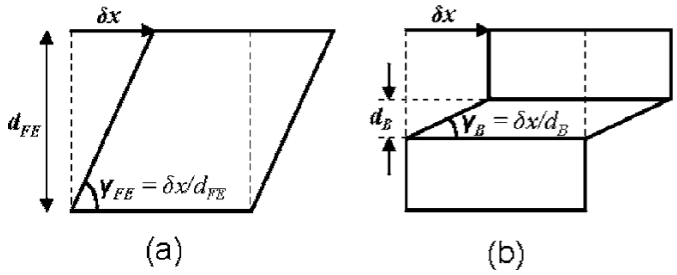

Figure 35. Idealized simple shear conditions: (a) finite-element computed shear strain; (b) shear strain along the shear band (Anastasopoulos et al. (2007))

The extra stress $\Delta\sigma_{peak}$ and $\Delta\sigma_{res}$ can be easily computed by one-element test analysis. Anastasopoulos et al. (2007) proposed such a methodology for calibrating the Mohr-Coulomb model, using a direct shear stress (Figure 35). According to this method, the plastic shear strain γ_{peak} corresponds to φ_{peak} and the γ_{res} corresponds to φ_{res} can be computed by Eq. 49 and Eq. 50 respectively.

$$\gamma_{peak} = \frac{\delta x_{peak} - \delta x_y}{D} \qquad \text{Eq. 49}$$

$$\gamma_{res} = \gamma_{peak} + \frac{\delta x_{res} - \delta x_{peak}}{d_{FE}} \qquad \text{Eq. 50}$$

In Eq. 49 and Eq. 50, D is the initial depth of the soil sample and d_{FE} the height of one-element test as shown in Figure 35a. A correction of peak angle of friction must be considered because of plane strain conditions as suggested by Jewell (1989) according to equation (9).

$$\sin(\varphi_{peak}^{PS}) = \frac{\tan(\varphi_{peak})}{\cos(\psi) + \sin(\psi)\tan(\varphi_{peak})} \qquad \text{Eq. 51}$$

where the φ_{peak}^{PS} is peak friction angle under the plane-strain conditions and ψ is the dilation angle, which is equal to $\varphi_{peak} - \varphi_{res}$.

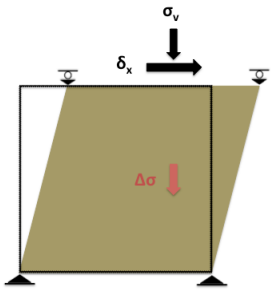

Figure 36. Schematic representation of one element model with restrict of the vertical deformation (δ_y=0) in order to compute the extra stress Δσ due to dilatancy of the sand.

In order to compute the extra stress Δσ, a restriction in the vertical movement of the one element model must be applied, as shown in Figure 36. From this procedure, the value of $\Delta\sigma_{peak}$ and the value of $\Delta\sigma_{res}$ can be obtained. This methodology was applied for axial tests conducted by CSM. The values of $\Delta\sigma_{peak}$ and $\Delta\sigma_{res}$ have been calculated equal to 12.5 kPa and 8.12 kPa for axial test 1 and 4.5 kPa and 0 kPa for axial test 2, respectively. A comparison between experimental results and the value of maximum soil resistance in the axial direction from Eq. 45 is illustrated in Figure 37 and Figure 38 for axial test 1 and axial test 2, respectively. The prediction of pipe-soil interaction using Eq. 45 provides very satisfactory results.

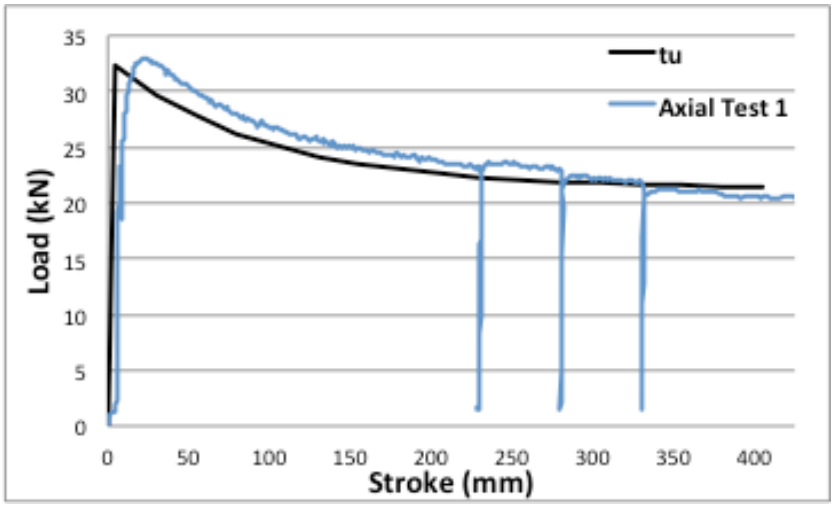

Figure 37. Comparison between Axial Test 1 conducted by CSM and the value of t_u by equation (3).

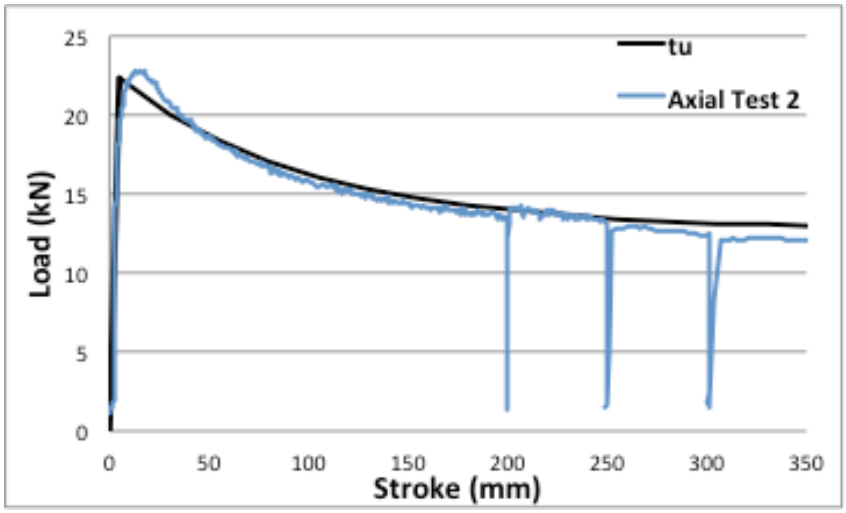

Figure 38. Comparison between Axial Test 2 conducted by CSM and the value of t_u by equation (3).

The finite element model that simulates the axial test (pull-out test) conducted by CSM is shown in Figure 39. The pipeline is pulled outwards at the near end, whereas the far end remains free. A contact algorithm has been developed in order to describe the pipe soil interaction using the user subroutine FRIC. The friction law described by equation (3) has been implemented in the FRIC subroutine in order to account for dilatancy of the sand.

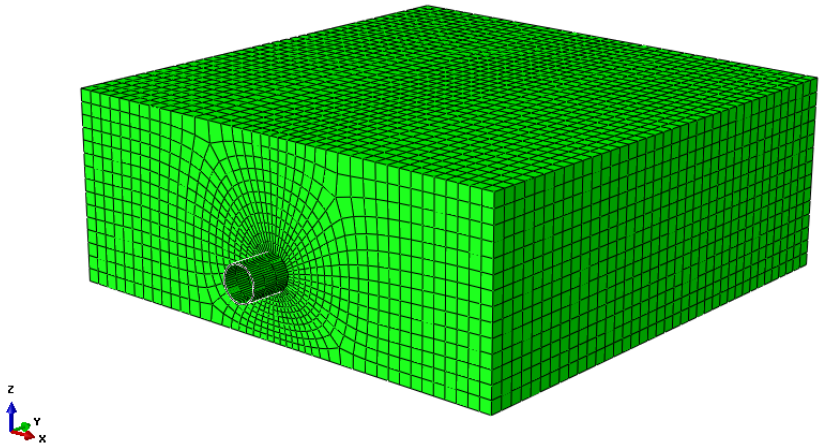

Figure 39. Finite Element model of pull out test contacted by CSM.

A comparison between experimental results and those from the finite element model described above is shown in Figure 40 and Figure 41 for axial test 1 and 2, respectively. The prediction of pipe-soil interaction as obtained from the finite

element model is very good. The conditions for axial test 3 are quite similar to those for test 1 except for the coating of the pipe. Figure 27 shows that the decay law from axial test 3 is different than the one in test 1 but the peak and residual values are quite similar. According to the above methodology the peak and the residual value can be predicted for axial test 3 with good accuracy but the decay rate cannot be predicted accurately.

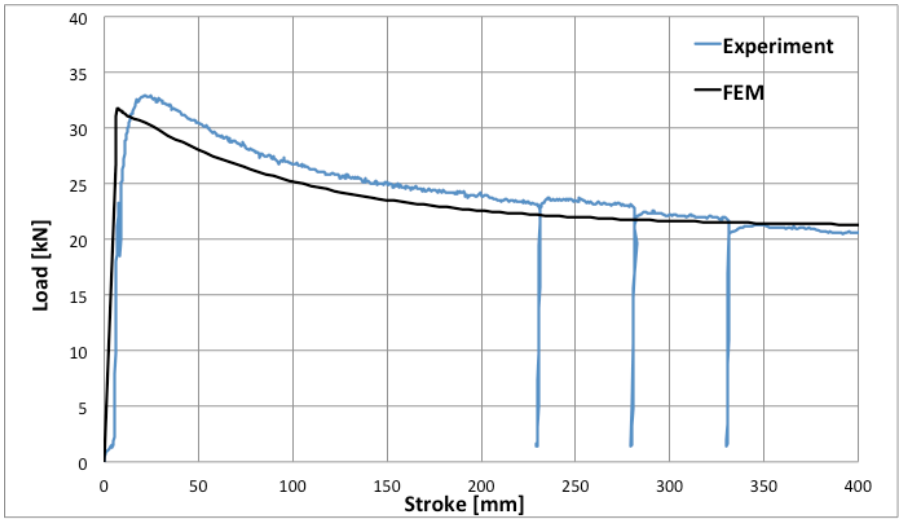

Figure 40. Comparison between the results of axial test 1 and the finite element predictions.

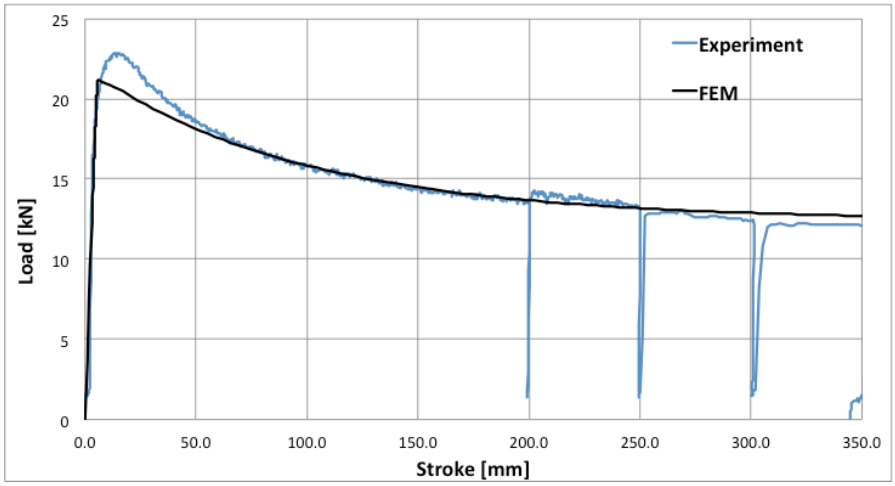

Figure 41. Comparison between the results of axial test 2 and the finite element predictions.

3.4 Simulation of landslide/fault test

Landslide tests have been performed by CSM in order to investigate the complex behavior of pipe-soil interaction in a special "landslide/fault" device. The experimental setup is shown in Figure 42 to Figure 45. The setup is composed by two fixed concrete boxes and one sliding box in-between as shown in Figure 42. The two ends of the pipe are free to move in the longitudinal direction during the test. The longitudinal strains measured by strain gauges for various displacement values of the middle box. A schematic representation of the deformed shape of the pipeline is shown in Figure 46.

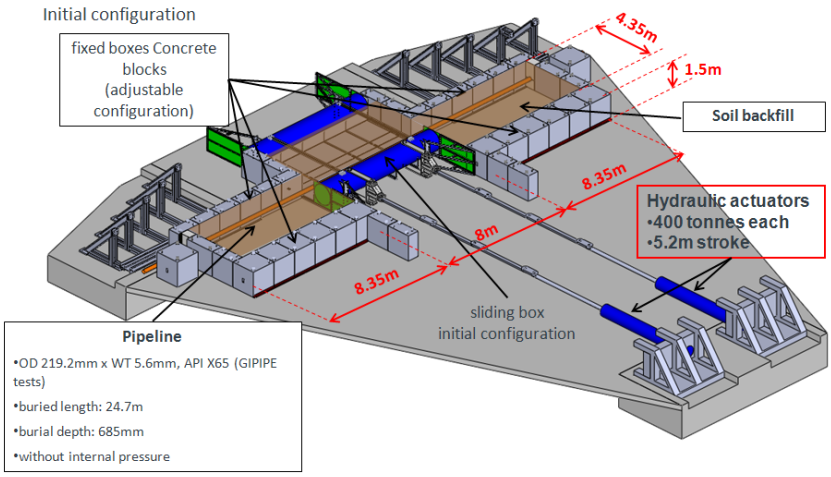

Figure 42. Schematic representation of experimental setup of tests in a landslide/fault device conducted by CSM.

Figure 43. Experimental setup of "landslide/fault" tests conducted by CSM.

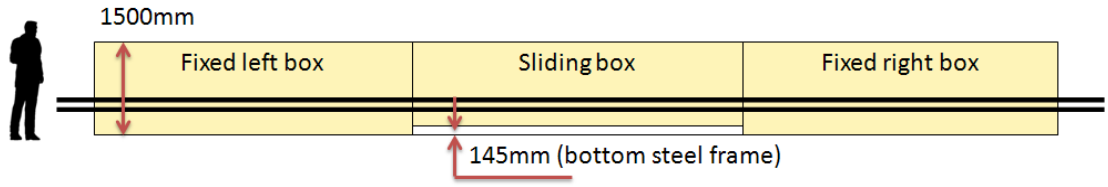

Figure 44. Internal box dimensions – lateral view.

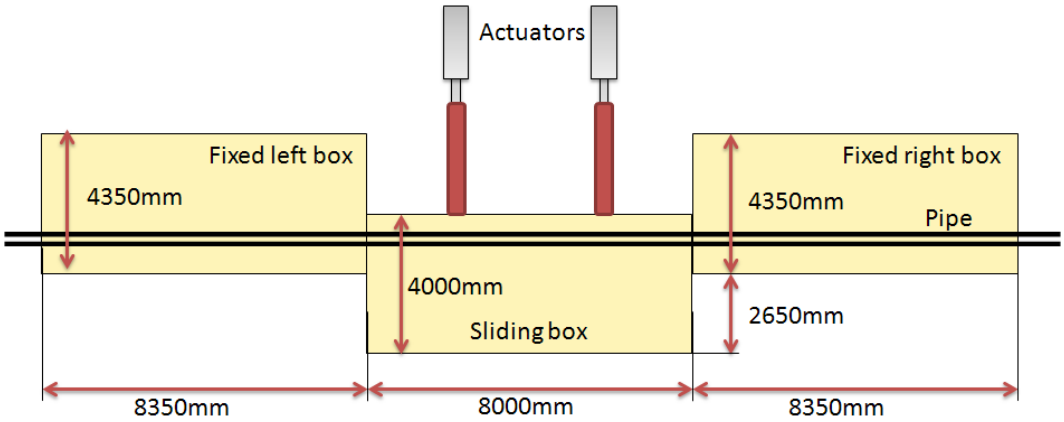

Figure 45. Internal box dimensions – plan view.

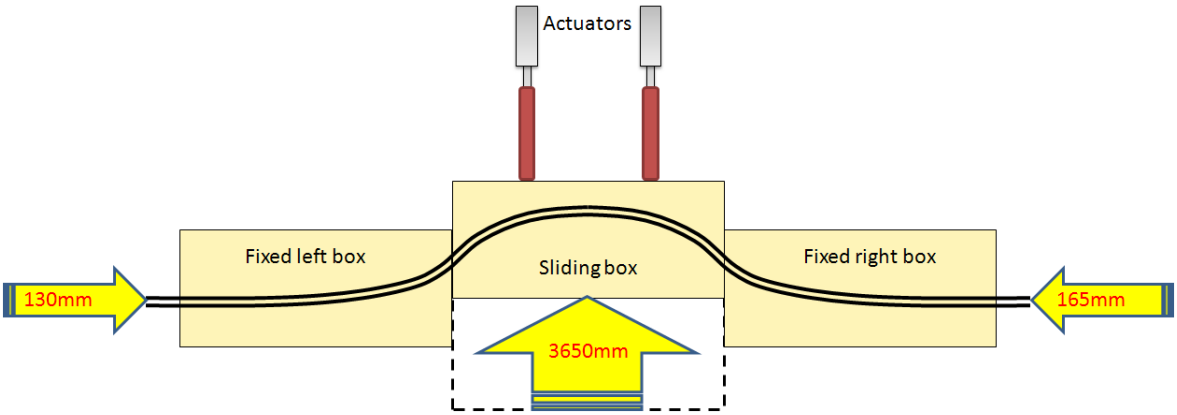

Figure 46. Sliding box and pipe-end displacements.

A finite element model has been developed, which simulates the "landslide/fault" tests. The model is shown in Figure 47. The middle box slides along the x axis as shown in Figure 47 while the two far boxes remain foxed. In Figure 48 and Figure 49 the deformed shape of pipe specimen from the first "landslide/fault" test is illustrated for box displacement equal to 229 mm (1.04 pipe diameters). The comparison between the experimental results and the finite element analysis results is shown in Figure 50, Figure 51 and Figure 52 for box displacement equal to 200, 400 and 600 mm, which is equal to 0.91, 1.82 and 2.74 pipe diameters, respectively. In Figure 50, Figure 51 and Figure 52 the longitudinal strains at the extrados with respect to the

pipe axis are shown along the half specimen. A difference in the position of the maximum strain was observed between numerical and experimental results. This difference is probably to the coarse mesh, which employed in order to reduce the computational effort. In any case more simulation will follow with a denser mesh not only for the landslide test 1, but also for the tests 2, 3 and 4 according to Table 6.

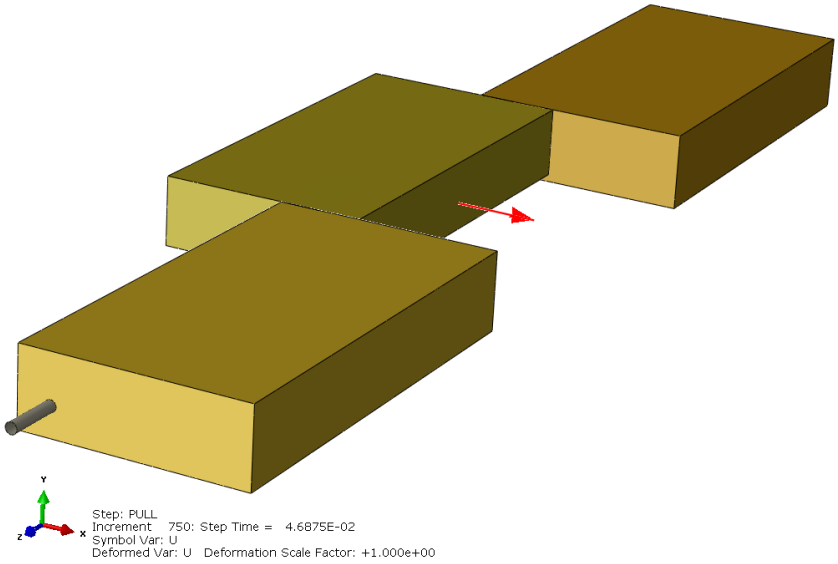

Figure 47. General configuration (solid model) of the simulation of CSM landslide/fault test.

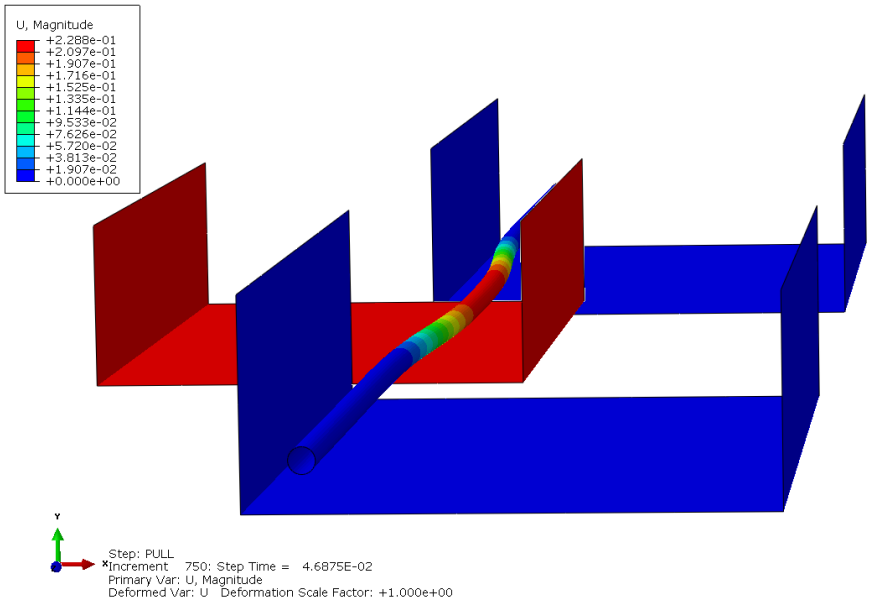

Figure 48. Deformed shape of the finite element model simulating “landslide/fault” test 1 corresponding to a value of box displacement equal to 229 mm (equal to1.05 pipe diameters).

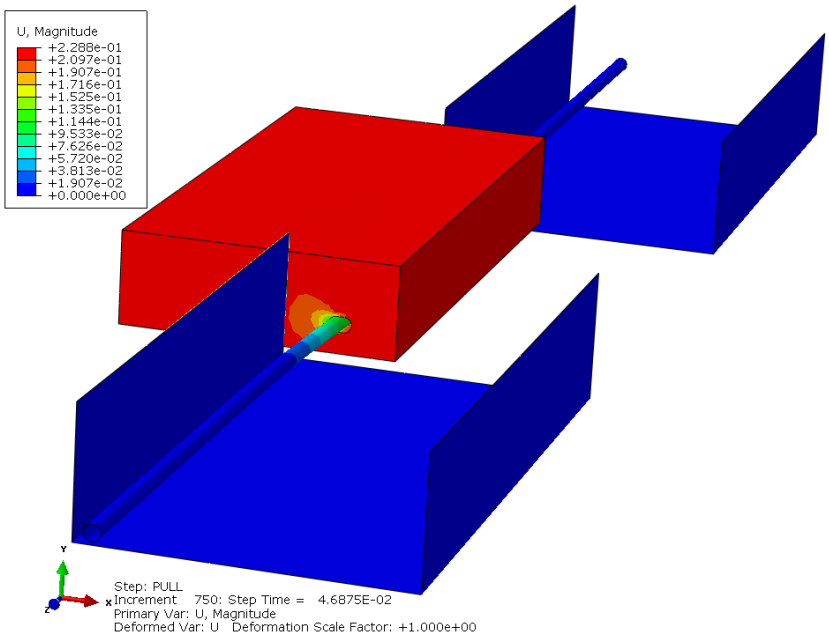

Figure 49. Deformed shape of the finite element model for the simulation of "landslide/fault" test 1 corresponding to a value of box displacement equal to 229 mm (equal to 1.05 pipe diameters).

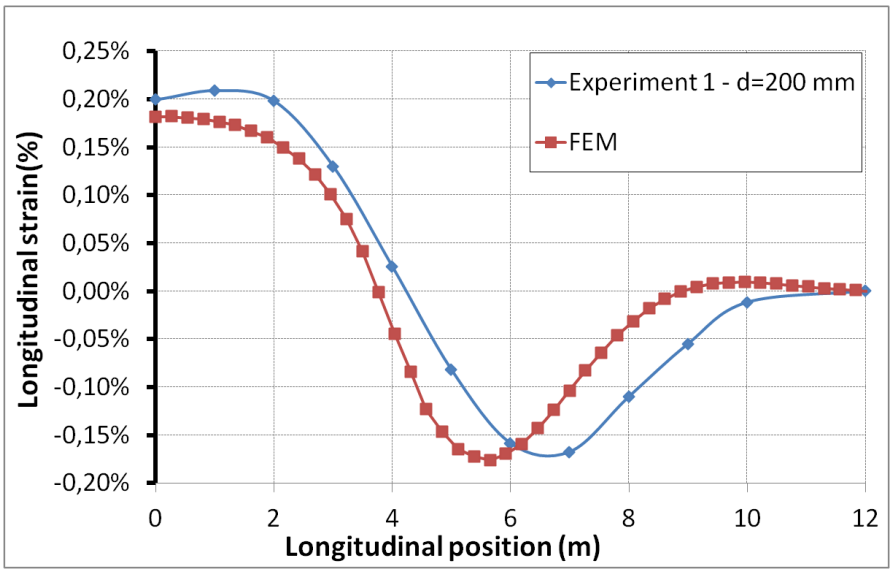

Figure 50. Comparison between landslide/fault test 1 results and finite element analysis in terms of the longitudinal strains along the pipe axis, for box displacement equal to 200 mm (equal to 0.91 pipe diameters).

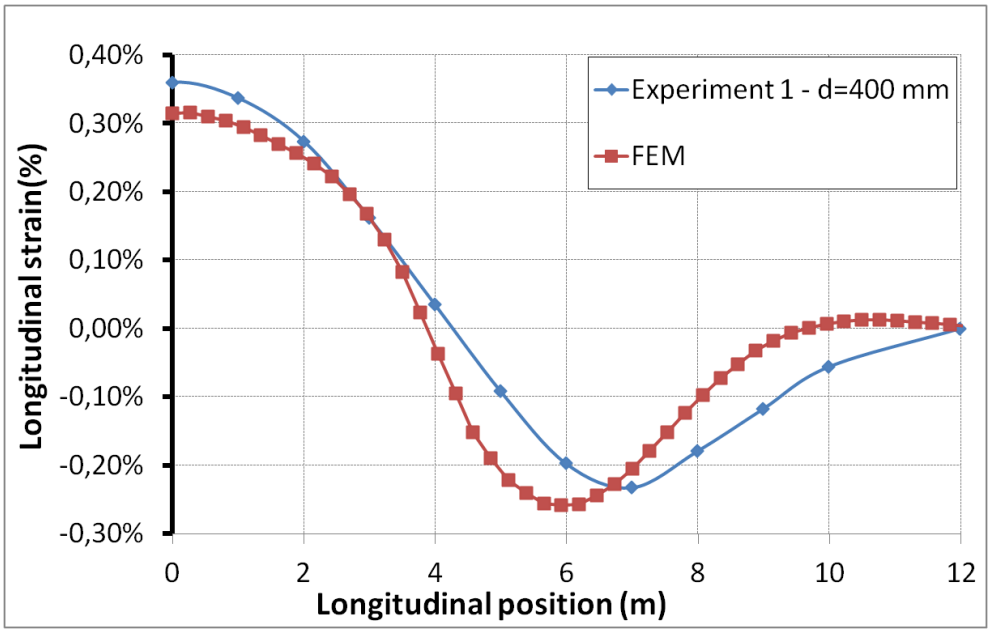

Figure 51. Comparison between landslide\fault test 1 results and finite element analysis in terms of the longitudinal strains along the pipe axis, for box displacement equal to 400 mm (equal to 1.82 pipe diameters).

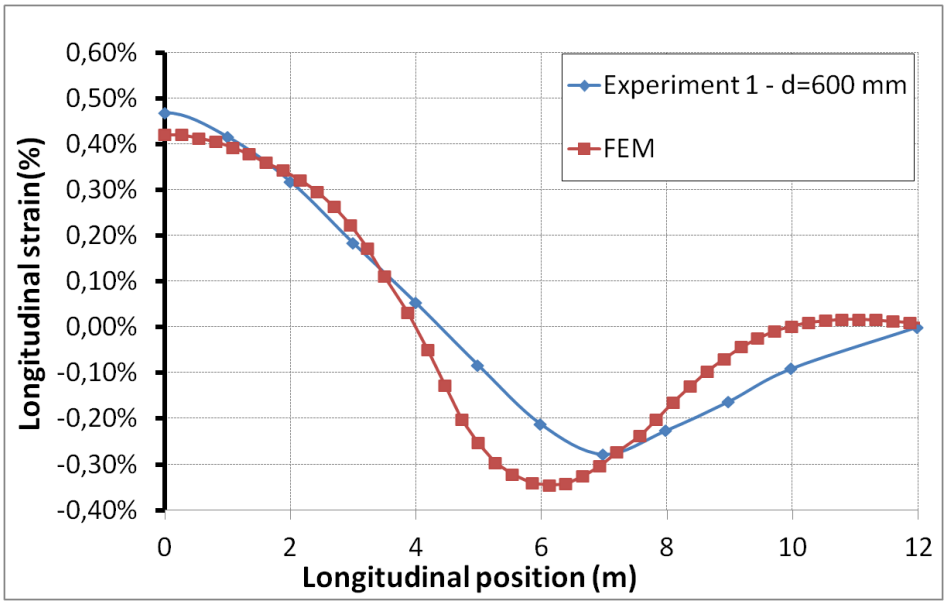

Figure 52. Comparison between landslide\fault test 1 results and finite element analysis in terms of the longitudinal strains along the pipe axis, for box displacement equal to 600 mm (equal to 2.74 pipe diameters).

4. Conclusions

Analytical and numerical methodologies for analyzing buried steel pipelines subjected to permanent seismic fault movement have been investigated. More specifically two analytical methodologies from the literature have been investigated while a new methodology for the calculation of the length of the deformed S-shape of the pipe has been developed and compared with finite element analysis. Moreover the pipe-soil interaction was investigated through the simulation of experimental tests, which conducted by CSM, in Sardinia.

The main conclusions derived from this study can be summarized as follows:

- A new analytical methodology for the calculation of the Length of the deformed S-shape of the pipeline for all types of faults was developed and compared to finite elements analysis. The results of the comparison were quite satisfactory.
- The calculation of the deformed Length of the pipeline was used in Vazouras et. al method in order to compute the strains of the pipeline in a case of a strike-slip fault. The results were compared with finite element analysis and the comparison was quite satisfactory.
- The Vazouras et. al method can be extended also for normal and oblique faults by using the methodology for the prediction of the Length of the deformed S-shape of the pipeline.
- The axial pipe-soil interaction was investigated:
    - In the case of a soil without dilatancy both the finite element model and the formula from the codes are in good agreement with the experimental results.
    - In the case of a soil with dilatancy the extra stress $\Delta\sigma$ due to dilatancy must be taken into account.
- A new axial spring was developed which takes into consideration the dilatancy and the softening of the soil.
- A contact algorithm was developed, using the subroutine FRIC of software Abaqus for 3D finite elements models, in order to take account of the extra stress $\Delta\sigma$ due to dilatancy of the soil.

- The transversal pipe-soil interaction was also investigated, the results from the finite element analysis are in good agreement with the experimental results.
- The pipe-soil interaction was investigated in a complex loading condition through the landslide test.

5. References

American Lifelines Alliance, (2001), Guidelines for the Design of Buried Steel Pipe.

Anastasopoulos I., Gazetas G., Bransby M.F., Davies M.C.R., El Nahas A. (2007), "Fault rupture propagation through sand: finite element analysis and validation through centrifuge experiments", *Journal of Geotechnical and Geoenvironmental Enineering, ASCE*, 133(8): 943–958.

Anastasopoulos I., Georgarakos T., Georgiannou V., Drosos V., Kourkoulis R. (2010), "Seismic Performance of Bar-Mat Reinforced-Soil Retaining Wall: Shaking Table Testing versus Numerical Analysis with Modified Kinematic Hardening Constitutive Model", *Soil Dynamics & Earthquake Engineering*, 30(10): 1089–1105.

ASCE. 1984, Guidelines for seismic design of oil and gas pipeline systems. Committee on Gas and Liquid Fuel Lifelines, Technical Council on Lifeline Earthquake Engineering, America Society of Civil Engineers, Reston, Va.

Comité Européen de Normalisation (2009), EN 1594 Gas supply systems – Pipelines for maximum operating pressure over 16 bar – Functional requirements, Brussels, Belgium.

Jewell, R. A., and Roth, C. P. (1987). "Direct shear tests on reinforced sand." *Geotechnique*, 37(1), 53–68.

Karimian, H. 2006. Response of buried steel pipelines subjected to longitudinal and transverse ground movement. Ph.D. thesis, De- partment of Civil Engineering, The University of British Colum- bia, Vancouver, B.C.

Karamitros, D. K., Bouckovalas, G. D., and Kouretzis, G. P. (2007), "Stress Analysis of Buried Steel Pipelines at Strike-Slip Fault Crossings.", *Soil Dynamics & Earthquake Engineering*, Vol. 27, pp. 200-211

Kennedy, R. P., Chow, A. W. and Williamson, R. A. (1977), "Fault movement effects on buried oil pipeline", *ASCE Journal of Transportation Engineering*, Vol. 103, pp. 617-633.

Nederlands Normalisatie-Instituut (2006), *Requirements for Pipeline Systems*, NEN 3650, Part-1: General, and Part-2: Steel Pipelines.

Newmark N. M., Hall W. J. (1975), "Pipeline design to resist large fault displacement". *Proceedings of U.S. National Conference on Earthquake Engineering*; 416–425.

Scarpelli, G., Sakellariadi, E., Furlani, G., Evaluation of soil-pipeline longitudinal interaction forces, Rivista Italiana di Geotecnica 4/2003

Takada, S., Hassani, N. and Fukuda, K. (2001), "A new proposal for simplified design of buried steel pipes crossing active faults", *Earthquake Engineering and Structural Dynamics*, 2001; Vol. 30: pp.1243–1257.

Trautmann, C.H., and O'Rourke, T.D. 1983. Behaviour of pipe in dry sand under lateral and uplift loading. Cornell University, Ithaca, N.Y. Geotechnical Engineering Report 83–7.

Trautmann, C.H. and O'Rourke, T.D, (1985), "Lateral Force-Displacement Response of Buried Pipe," Journal of Geotechnical Engineering, ASCE, Vol.111, No.9, pp.1077-1092.

Trifonov, O. V. and Cherniy, V. P. (2010), "A semi-analytical approach to a nonlinear stress–strain analysis of buried steel pipelines crossing active faults.", *Soil Dynamics & Earthquake Engineering*, Vol. 30, pp. 1298-1308.

Trifonov, O. V. and Cherniy, V. P. (2012), "Elastoplastic stress-strain analysis of buried steel pipelines subjected to fault displacements with account for service loads.", *Soil Dynamics & Earthquake Engineering*, Vol. 33, No. 1, pp. 54-62.

Vazouras, P., Karamanos, S. A., and Dakoulas, P. (2010), "Finite Element Analysis of Buried Steel Pipelines Under Strike-Slip Fault Displacements", *Soil Dynamics and Earthquake Engineering*, Vol. 30, No. 11, pp. 1361–1376.

Vazouras, P., Karamanos, S. A., and Dakoulas, P. (2012), "Mechanical behavior of buried steel pipes crossing active strike-slip faults", *Soil Dynamics and Earthq. Engineering*, 41:164–180.

Vazouras, P., Dakoulas, P., and Karamanos, S. A. (2015), "Pipe-Soil Interaction and Pipeline Performance Under Strike-Slip Fault Movements.", Soil Dynamics & Earthquake Engineering

Vardoulakis I., and Graf B. (1985). "Calibration of constitutive models for granular materials using data from biaxial experiments." *Geotechnique*, 35(3), 299–317.

Wang, L. R. L. and Yeh, Y. A. (1985), "A refined seismic analysis and design of buried pipeline for fault movement", *Earthquake Engineering & Structural Dynamics*, Vol. 13, pp. 75-96.

Wang L. L. R., Wang L. J. (1995), Parametric study of buried pipelines due to large fault movement. *ASCE, TCLEE* 1995; (6):152–159.